

UNIFORMLY ACCURATE METHODS FOR THREE DIMENSIONAL VLASOV EQUATIONS UNDER STRONG MAGNETIC FIELD WITH VARYING DIRECTION

PHILIPPE CHARTIER, NICOLAS CROUSEILLES, MOHAMMED LEMOU, FLORIAN MÉHATS,
AND XIAOFEI ZHAO

ABSTRACT. In this paper, we consider the three dimensional Vlasov equation with an inhomogeneous, varying direction, strong magnetic field. Whenever the magnetic field has constant intensity, the oscillations generated by the stiff term are periodic. The homogenized model is then derived and several state-of-the-art multiscale methods, in combination with the Particle-In-Cell discretisation, are proposed for solving the Vlasov-Poisson equation. Their accuracy as much as their computational cost remain essentially independent of the strength of the magnetic field. The proposed schemes thus allow large computational steps, while the full gyro-motion can be restored by a linear interpolation in time. In the linear case, extensions are introduced for general magnetic field (varying intensity and direction). Eventually, numerical experiments are exposed to illustrate the efficiency of the methods and some long-term simulations are presented.

Keywords: Vlasov-Poisson equation, Three dimensions, Strong magnetic field, Varying direction, Uniformly accurate method, Particle-In-Cell.

AMS Subject Classification: 65L05, 65L20, 65L70.

1. INTRODUCTION

Vlasov models have been widely considered for modelling the dynamics of plasmas as encountered in magnetic fusion devices known as a tokamaks, where a strong external magnetic field is applied so as to confine the charged particles. In this paper, we consider the three dimensional Vlasov-Poisson equation with a strong non-homogeneous magnetic field whose direction may vary [16, 24, 35]

$$\partial_t f^\varepsilon(t, \mathbf{x}, \mathbf{v}) + \mathbf{v} \cdot \nabla_{\mathbf{x}} f^\varepsilon(t, \mathbf{x}, \mathbf{v}) + \left(\mathbf{E}(t, \mathbf{x}) + \frac{1}{\varepsilon} \mathbf{v} \times \mathbf{B}(\mathbf{x}) \right) \cdot \nabla_{\mathbf{v}} f^\varepsilon(t, \mathbf{x}, \mathbf{v}) = 0, \quad (1.1a)$$

$$\nabla_{\mathbf{x}} \cdot \mathbf{E}(t, \mathbf{x}) = \int_{\mathbb{R}^3} f^\varepsilon(t, \mathbf{x}, \mathbf{v}) d\mathbf{v} - n_i, \quad (1.1b)$$

$$f^\varepsilon(0, \mathbf{x}, \mathbf{v}) = f_0(\mathbf{x}, \mathbf{v}), \quad (1.1c)$$

where, for a given $T > 0$,

$$f^\varepsilon : (t, \mathbf{x}, \mathbf{v}) \in [0, T] \times \mathbb{R}^3 \times \mathbb{R}^3 \mapsto f^\varepsilon(t, \mathbf{x}, \mathbf{v}) \in \mathbb{R}$$

is the unknown,

$$f_0 : (\mathbf{x}, \mathbf{v}) \in \mathbb{R}^3 \times \mathbb{R}^3 \mapsto f_0(\mathbf{x}, \mathbf{v}) \in \mathbb{R}$$

a given initial distribution, where

$$\mathbf{B} : \mathbf{x} \in \mathbb{R}^3 \mapsto \mathbf{B}(\mathbf{x}) \in \mathbb{R}^3$$

denotes the external magnetic field,

$$\mathbf{E} : (t, \mathbf{x}) \in \mathbb{R}^+ \times \mathbb{R}^3 \mapsto \mathbf{E}(t, \mathbf{x}) \in \mathbb{R}^3$$

the self-consistent electric-field function, $0 < \varepsilon \leq 1$ a dimensionless parameter inversely proportional to the strength of the magnetic field and $n_i \geq 0$ the ion density of the background. The system (1.1) has a lot of invariants and we will be interested in particular in the Hamiltonian defined by

$$\mathcal{H}(t) := \int_{\mathbb{R}^3} \int_{\mathbb{R}^3} \frac{1}{2} |\mathbf{v}|^2 f^\varepsilon(t, \mathbf{x}, \mathbf{v}) d\mathbf{x} d\mathbf{v} + \frac{1}{2} \int_{\mathbb{R}^3} |\mathbf{E}(t, \mathbf{x})|^2 d\mathbf{x}. \quad (1.2)$$

The above Vlasov-Poisson model (1.1) is derived from the three dimensional Vlasov-Maxwell equations by considering the electrostatic approximation. Unlike some asymptotically reduced models such as the gyrokinetic equations [29, 33] or the drift-kinetic limit equations [3, 22, 18], model (1.1) is set at the kinetic scale and is of paramount importance for studying the plasma dynamics in the tokamak device.

In the strong magnetic field limit regime, the charged particles exhibit very fast rotations with cyclotron period proportional to ε , while remaining confined along the magnetic line. In such a case, the small parameter $0 < \varepsilon \ll 1$ renders the solution $f^\varepsilon(t, \mathbf{x}, \mathbf{v})$ of (1.1) highly-oscillatory in time. Classical numerical integrators such as splitting or finite-difference schemes thus require time steps smaller than the cyclotron period in order to accurately capture the dynamics, thus implying severe computational burden. Recent efforts have aimed at designing numerical schemes which allow step-sizes much larger than the cyclotron period. Upon assuming that the magnetic field has a fixed direction in space, i.e. that

$$\mathbf{B}(\mathbf{x}) = (0, 0, b(\mathbf{x}))^T, \quad b(\mathbf{x}) > 0$$

(a popular choice both for formal and rigorous analyses [3, 16, 24]), several multiscale numerical methods have been proposed [10, 15, 17, 19, 20, 23]. Among them, Filbet et al. constructed Particle-In-Cell schemes in the spirit of asymptotic preserving techniques [27], which, as $\varepsilon \rightarrow 0$, are consistent with the drift-limit model [19] or the gyrokinetic model [17, 20]. These schemes are simple and highly accurate, but the gyro-motion is lost in the limit regime. In contrast, the schemes proposed in [10, 15] capture all the information of the kinetic models with an accuracy uniform with respect to $0 < \varepsilon \leq 1$. These *uniformly accurate (UA)* schemes have computational cost as well as accuracy totally independent of ε (we refer to [14] for a comparison of UA scheme with other multiscale methods). In order to design UA schemes for kinetic models, different numerical approaches may be used: (i) The two-scale formulation technique relies upon an explicit separation of the fast and slow times and allows to smooth out the oscillations [10, 13, 15]. (ii) The multi-revolution composition methods, in the spirit of heterogeneous multiscale method [1], are also UA, as confirmed in the recent paper [11]. Both approaches exploit the periodicity of the solution of the stiff part of the equation. For instance, our recent work [10] isolates the dominant oscillation frequency owing to a confining property in two dimensions. However, the general case of a strong magnetic field with varying direction, i.e.

$$\mathbf{B}(\mathbf{x}) = (b_1(\mathbf{x}), b_2(\mathbf{x}), b_3(\mathbf{x}))^T,$$

has been barely considered so far for the Vlasov-Poisson equation (1.1) due to its complicated highly-oscillatory behaviour in three dimensions. Let us also mention recent developments around symplectic Particle-In-Cell method, which allows for good preservation of invariants for very long time (see [25, 32, 28]).

In this work, we propose efficient numerical schemes for solving the three dimensional Vlasov-Poisson equation (1.1) in the strong magnetic field regime by combining multiscale strategies with the Particle-In-Cell (PIC) discretisation. First, we consider the case of a magnetic field with constant intensity $|\mathbf{B}(\mathbf{x})| = \text{const}$, for which, as already pointed out in [5, 33], the motion induced by the stiff Lorentz term $\frac{1}{\varepsilon} \mathbf{v} \times \mathbf{B}(\mathbf{x})$ in (1.1) is periodic in time. Taking advantage of this observation, we derive the limit model of (1.1) by using averaging methods [5], and then introduce three UA schemes, namely (i) the multi-revolution composition (MRC) method, (ii) the two-scale formulation (TSF) method and (iii) the micro-macro (MM) method. All three are of uniform second order in time for all $\varepsilon \in]0, 1]$, though have specific pros and cons: for instance, MRC methods are phase-space volume preserving, while MM easily allows for the full recovery of the gyro-motion. To the best of our knowledge, this key-feature is new and paves the way for an extension to the case of a magnetic field with varying intensity. In this situation, we indeed introduce, under the PIC discretisation, a reparametrization of time to re-normalise the magnetic field. Within this framework, each particle carries its own fictitious time. Hence, and in order to avoid the occurrence of multiple frequencies, we drop in this situation the Poisson part of (1.1) and consider instead the case of an external electric field $\mathbf{E}(t, \mathbf{x})$ (this somehow simplifying assumption is relevant as it marks an important first step towards the solution of the full problem). In order to re-synchronise all particles (a necessary

step in order to provide an approximation of $f^\varepsilon(t, \mathbf{x}, \mathbf{v})$), we then use the interpolation strategy of MM which ensures uniform second order except for the angular variable. Eventually, numerical experiments are presented in order to validate uniform accuracy and to compare the various methods. In particular, we simulate the dynamics of equation (1.1) in a three dimensional screw-pinch setup [29].

The remaining of the paper is now organized as follows. Section 2 considers the limit model of (1.1) with a constant intensity $\mathbf{B}(\mathbf{x})$ and Section 3 introduces the three aforementioned UA schemes in this situation: Subsection 3.1 is concerned with MRC method, Subsection 3.2 with TSF method and Subsection 3.3 with MM method. Extensions to the case of a varying intensity are presented in Section 4. Finally, numerical results with concluding remarks are exposed in Section 5.

2. AVERAGING

A general assumption throughout this paper is that the magnetic field is bounded from below, i.e. that $|\mathbf{B}(\mathbf{x})| \geq c_0$ for all $\mathbf{x} \in \mathbb{R}^3$ for some $c_0 > 0$ independent of ε . In this section, we further assume that the external magnetic field has constant norm

$$|\mathbf{B}(\mathbf{x})| \equiv \text{const} > 0, \quad \mathbf{x} \in \mathbb{R}^3,$$

so that the stiff part of equation (1.1) generates periodic motion. This setup has also been considered in [24]. A possible instance of such a \mathbf{B} is given by $\mathbf{B}(\mathbf{x}) = (B_1(x_1, x_2), B_2(x_1, x_2), B_3(x_1, x_2))$ where

$$B_3 = \sqrt{\|B_1^2 + B_2^2\|_{L^\infty(\mathbb{R}^2)} - B_1^2 - B_2^2},$$

with $(B_1(x_1, x_2), B_2(x_1, x_2)) \in L^\infty(\mathbb{R}^2)$ and $\partial_{x_1} B_1 + \partial_{x_2} B_2 = 0$. It can be verified that $|\mathbf{B}(\mathbf{x})|^2 \equiv \|B_1^2 + B_2^2\|_{L^\infty(\mathbb{R}^2)}$ and $\nabla_x \cdot \mathbf{B} \equiv 0$. In such a case, we are able to apply a recently developed averaging method to quickly obtain the limit model of (1.1) as $\varepsilon \rightarrow 0$.

Lemma 2.1. *If $|\mathbf{B}(\mathbf{x})| \equiv b$ for some constant $b > 0$, then the solution of*

$$\partial_t \tilde{f}^\varepsilon(t, \mathbf{x}, \mathbf{v}) + \frac{1}{\varepsilon} \mathbf{v} \times \mathbf{B}(\mathbf{x}) \cdot \nabla_{\mathbf{v}} \tilde{f}^\varepsilon(t, \mathbf{x}, \mathbf{v}) = 0, \quad (2.1)$$

is $2\pi/b$ -periodic with respect to the fast time-variable t/ε .

Proof. The characteristics of (2.1)

$$\dot{\mathbf{x}}(t) = 0, \quad \dot{\mathbf{v}}(t) = \frac{1}{\varepsilon} \mathbf{v}(t) \times \mathbf{B}(\mathbf{x}(t)), \quad t > 0,$$

have a periodic solution in t/ε which can be obtained, for instance, by Rodrigues' formula

$$\begin{aligned} \mathbf{x}(t) &= \mathbf{x}(0), \\ \mathbf{v}(t) &= \cos(bt/\varepsilon) \mathbf{v}(0) + (1 - \cos(bt/\varepsilon)) (\mathbf{B}(\mathbf{x}(0)) \cdot \mathbf{v}(0)) \mathbf{B}(\mathbf{x}(0)) - \sin(bt/\varepsilon) \mathbf{v}(0) \times \mathbf{B}(\mathbf{x}(0)). \end{aligned} \quad (2.2)$$

The statement of the lemma is now an immediate consequence. \square

Using the observation above, we may apply the following theorem from [5]:

Theorem 2.2. *Consider a transport equation of form*

$$\partial_t f^\varepsilon(t, \mathbf{y}) + \left[\frac{G(\mathbf{y})}{\varepsilon} + K(\mathbf{y}) \right] \cdot \nabla_{\mathbf{y}} f^\varepsilon(t, \mathbf{y}) = 0, \quad f^\varepsilon(0, \mathbf{y}) = f_0(\mathbf{y}),$$

where the flow map Φ_t of

$$\dot{\mathbf{y}}(t) = G(\mathbf{y}(t))$$

is assumed to be 2π -periodic. There exist two formal vector fields $G^\varepsilon(\mathbf{y})$ and $K^\varepsilon(\mathbf{y})$ satisfying

$$\frac{G(\mathbf{y})}{\varepsilon} + K(\mathbf{y}) = \frac{G^\varepsilon(\mathbf{y})}{\varepsilon} + K^\varepsilon(\mathbf{y}) \quad \text{and} \quad [G^\varepsilon, K^\varepsilon] = 0,$$

such that the system

$$\begin{cases} \partial_\tau g(t, \tau, \mathbf{y}) + G^\varepsilon(\mathbf{y}) \cdot \nabla_{\mathbf{y}} g(t, \tau, \mathbf{y}) = 0, & (2.3a) \\ \partial_t g(t, \tau, \mathbf{y}) + K^\varepsilon(\mathbf{y}) \cdot \nabla_{\mathbf{y}} g(t, \tau, \mathbf{y}) = 0, & (2.3b) \\ g(0, 0, \mathbf{y}) = f_0(\mathbf{y}). & (2.3c) \end{cases}$$

has a unique formal solution independently of the order in which the equations are solved. Moreover, for all positive time we have $f^\varepsilon(t, \mathbf{y}) = g(t, t/\varepsilon, \mathbf{y})$ and the first two terms of $K^\varepsilon = K^{[1]} + \varepsilon K^{[2]} + O(\varepsilon^2)$ may be computed as follows

$$K^{[1]} = \Pi K_\tau, \quad K^{[2]} = -\frac{1}{2}\Pi \int_0^\tau [K_s, K_\tau] ds, \quad \text{with} \quad K_\tau(\mathbf{y}) := (D_{\mathbf{y}}\Phi_\tau(\mathbf{y}))^{-1} (K \circ \Phi_\tau)(\mathbf{y}),$$

with $\Pi h := 1/(2\pi) \int_0^{2\pi} h(\tau) d\tau$.

Remark 2.3. If K^ε is truncated at order k in ε and $G^\varepsilon = G(\mathbf{y}) + \varepsilon K(\mathbf{y}) - \varepsilon K^\varepsilon$, then the order in which the equations in (2.3) are solved does matter. However, the difference between the corresponding two solutions is also of order ε^k .

Without loss of generality, we assume in the rest of this section that $|\mathbf{B}(\mathbf{x})| \equiv 1$ to derive the averaged model of equation (1.1) as obtained from Theorem 2.2. Details of the derivation may be found in [5] and we thus content ourselves with a sketch of the computations: from (1.1), we have

$$G = \begin{pmatrix} \mathbf{0} \\ \mathbf{v} \times \mathbf{B} \end{pmatrix}, \quad K = \begin{pmatrix} \mathbf{v} \\ \mathbf{E} \end{pmatrix},$$

and the flow map generated by G is given by

$$\Phi_\tau(\mathbf{y}) = \begin{pmatrix} \mathbf{x} \\ \cos(\tau)\mathbf{v} + \sin(\tau)\mathbf{v} \times \mathbf{B} + (1 - \cos(\tau))(\mathbf{B} \cdot \mathbf{v})\mathbf{B} \end{pmatrix}, \quad \mathbf{y} = \begin{pmatrix} \mathbf{x} \\ \mathbf{v} \end{pmatrix}.$$

Then

$$D_{\mathbf{y}}\Phi_\tau(\mathbf{y}) = \begin{pmatrix} I_3 & \mathbf{0} \\ N_1 & N_2 \end{pmatrix},$$

where

$$N_1 = \sin(\tau) (\mathbf{v} \times \nabla_{\mathbf{x}}\mathbf{B}) + (1 - \cos(\tau))[(\mathbf{B} \cdot \mathbf{v})\nabla_{\mathbf{x}}\mathbf{B} + \mathbf{B}(\mathbf{v}^T \nabla_{\mathbf{x}}\mathbf{B})],$$

$$N_2 = \cos(\tau)I_3 - \sin(\tau)(\mathbf{B} \times I_3) + (1 - \cos(\tau))\mathbf{B}\mathbf{B}^T$$

where we have denoted $\mathbf{v} \times \nabla_{\mathbf{x}}\mathbf{B} = [\mathbf{v} \times \partial_{x_1}\mathbf{B}, \mathbf{v} \times \partial_{x_2}\mathbf{B}, \mathbf{v} \times \partial_{x_3}\mathbf{B}]$ and similarly for $\mathbf{v} \times I_3$. A straightforward calculation then leads to

$$\Pi((D_{\mathbf{y}}\Phi_\tau(\mathbf{y}))^{-1}(K \cdot \Phi_\tau)) = \begin{pmatrix} (\mathbf{B} \cdot \mathbf{v})\mathbf{B} \\ \mathbf{B}_{\mathbf{v}} \end{pmatrix}$$

where

$$\mathbf{B}_{\mathbf{v}} = \mathbf{B}\mathbf{B}^T \left[\mathbf{E} - \frac{1}{2}(\mathbf{v} \times \nabla_{\mathbf{x}}\mathbf{B})(\mathbf{v} \times \mathbf{B}) + M\mathbf{v} - \frac{5}{2}M(\mathbf{B} \cdot \mathbf{v})\mathbf{B} \right] - \frac{1}{2}M[\mathbf{v} - 2(\mathbf{B} \cdot \mathbf{v})\mathbf{B}]$$

$$- \frac{1}{2}\mathbf{B} \times I_3 [M(\mathbf{v} \times \mathbf{B}) + (\mathbf{v} \times \nabla_{\mathbf{x}}\mathbf{B})(\mathbf{B} \cdot \mathbf{v})\mathbf{B}],$$

with

$$M = (\mathbf{B} \cdot \mathbf{v})\nabla_{\mathbf{x}}\mathbf{B} + \mathbf{B}(\mathbf{v}^T \nabla_{\mathbf{x}}\mathbf{B}).$$

Eventually,

$$K^\varepsilon = \begin{pmatrix} (\mathbf{B} \cdot \mathbf{v})\mathbf{B} \\ \mathbf{B}_{\mathbf{v}} \end{pmatrix} + O(\varepsilon),$$

and limit model at leading order is

$$\partial_t g(t, \tau, \mathbf{x}, \mathbf{v}) + (\mathbf{B} \cdot \mathbf{v})\mathbf{B} \cdot \nabla_{\mathbf{x}}g(t, \tau, \mathbf{x}, \mathbf{v}) + \mathbf{B}_{\mathbf{v}} \cdot \nabla_{\mathbf{v}}g(t, \tau, \mathbf{x}, \mathbf{v}) = 0, \quad t > 0.$$

By taking $\tau = 0$ and $f(t, \mathbf{x}, \mathbf{v}) = g(t, 0, \mathbf{x}, \mathbf{v})$, we get the leading order averaged model of (1.1) for stroboscopic times $t \in 2\pi\varepsilon\mathbb{N}$,

$$\partial_t f(t, \mathbf{x}, \mathbf{v}) + (\mathbf{B} \cdot \mathbf{v})\mathbf{B} \cdot \nabla_{\mathbf{x}}f(t, \mathbf{x}, \mathbf{v}) + \mathbf{B}_{\mathbf{v}} \cdot \nabla_{\mathbf{v}}f(t, \mathbf{x}, \mathbf{v}) = 0, \quad (2.4a)$$

$$\nabla_{\mathbf{x}} \cdot \mathbf{E}(t, \mathbf{x}) = \int_{\mathbb{R}^3} f(t, \mathbf{x}, \mathbf{v}) d\mathbf{v} - n_i, \quad (2.4b)$$

$$f(0, \mathbf{x}, \mathbf{v}) = f_0(\mathbf{x}, \mathbf{v}). \quad (2.4c)$$

As we shall verify later numerically, we have

$$f^\varepsilon(t, \mathbf{x}, \mathbf{v}) - f(t, \mathbf{x}, \mathbf{v}) = O(\varepsilon), \quad 0 < \varepsilon \ll 1, \quad t \in 2\pi\varepsilon\mathbb{N}.$$

3. NUMERICAL METHOD

In this section, we introduce numerical schemes for equation (1.1) under the assumption $|\mathbf{B}(\mathbf{x})| \equiv 1$. Taking advantage of the periodicity the solution of the stiff part, we apply state-of-art multiscale approaches in combination with PIC discretisation. In this way, we obtain schemes whose accuracy and computational cost are both independent of $\varepsilon \in]0, 1]$. Our starting point is the following PIC-representation of f^ε as used in, e.g., [19, 23, 26, 35],

$$f^\varepsilon(t, \mathbf{x}, \mathbf{v}) \approx \sum_{k=1}^{N_p} \omega_k \delta(\mathbf{x} - \mathbf{x}_k(t)) \delta(\mathbf{v} - \mathbf{v}_k(t)), \quad t \geq 0, \quad \mathbf{x}, \mathbf{v} \in \mathbb{R}^2. \quad (3.1)$$

The characteristic equations of model (1.1) for $1 \leq k \leq N_p$ are then of the form

$$\dot{\mathbf{x}}_k(t) = \mathbf{v}_k(t), \quad (3.2a)$$

$$\dot{\mathbf{v}}_k(t) = \mathbf{E}(t, \mathbf{x}_k(t)) + \frac{1}{\varepsilon} \mathbf{v}_k(t) \times \mathbf{B}(\mathbf{x}_k(t)), \quad t > 0, \quad (3.2b)$$

$$\mathbf{x}_k(0) = \mathbf{x}_{k,0}, \quad \mathbf{v}_k(0) = \mathbf{v}_{k,0}. \quad (3.2c)$$

Noticing that

$$\nabla_{\mathbf{x}} \cdot \mathbf{E}(t, \mathbf{x}) = \sum_{k=1}^{N_p} \omega_k \delta(\mathbf{x} - \mathbf{x}_k(t)),$$

we observe that the electric field \mathbf{E} in (3.2) has in fact no explicit dependence on time, i.e. $\mathbf{E}(t, \mathbf{x}) = \mathbf{E}_{[X(t)]}(\mathbf{x})$ where $X(t) = (\mathbf{x}_1(t), \dots, \mathbf{x}_{N_p}(t))$. We are in a position to briefly present three different UA methods.

3.1. Multi-revolution composition method. For a general exposition of multi-revolution composition (MRC), we refer to [8]. Here, we focus on a uniformly accurate second-order method.

MRC framework. Suppose that we wish to solve equation (1.1) on $[0, T_f]$ for some $T_f > 0$. Rescaling time in (3.2) leads to (we omit the particle index for brevity)

$$\dot{\mathbf{x}}(t) = \varepsilon \mathbf{v}(t), \quad (3.3a)$$

$$\dot{\mathbf{v}}(t) = \varepsilon \mathbf{E}_{[X(t)]}(\mathbf{x}(t)) + \mathbf{v}(t) \times \mathbf{B}(\mathbf{x}(t)), \quad 0 < t \leq \frac{T_f}{\varepsilon}, \quad (3.3b)$$

$$\mathbf{x}(0) = \mathbf{x}_0, \quad \mathbf{v}(0) = \mathbf{v}_0, \quad (3.3c)$$

Since the stiff part of (3.3) generates a 2π -periodic motion, equation (3.3) is amenable to MRC [8, 9]. To do so, we write

$$\frac{T_f}{\varepsilon} = 2\pi M_f + T_r, \quad M_f = \lfloor \frac{T_f}{2\pi\varepsilon} \rfloor \in \mathbb{N}, \quad 0 \leq T_r < 2\pi. \quad (3.4)$$

The 2nd order MRC method begins by choosing an integer $0 < M_0 \leq M_f$ and defining

$$\alpha = \frac{1}{2} \left(1 + \frac{1}{M_0} \right), \quad \beta = \frac{1}{2} \left(1 - \frac{1}{M_0} \right), \quad M = \frac{M_f}{M_0}, \quad H = \varepsilon M_0. \quad (3.5)$$

Denoting $\mathbf{x}^n \approx \mathbf{x}(2\pi n M_0)$, $\mathbf{v}^n \approx \mathbf{v}(2\pi n M_0)$, the MRC scheme proceeds as follows

$$\begin{pmatrix} \mathbf{x}^{n+1} \\ \mathbf{v}^{n+1} \end{pmatrix} = \mathcal{E}_\beta(-2\pi) \mathcal{E}_\alpha(2\pi) \begin{pmatrix} \mathbf{x}^n \\ \mathbf{v}^n \end{pmatrix}, \quad 0 \leq n \leq M - 1, \quad (3.6)$$

where $\mathcal{E}_\alpha(2\pi)$ denotes the value at time 2π of the flow of

$$\begin{cases} \dot{\mathbf{x}}(t) = \alpha H \mathbf{v}(t), \\ \dot{\mathbf{v}}(t) = \alpha H \mathbf{E}_{[X(t)]}(\mathbf{x}(t)) + \mathbf{v}(t) \times \mathbf{B}(\mathbf{x}(t)), \end{cases} \quad (3.7)$$

and $\mathcal{E}_\beta(-2\pi)$ the value at time (-2π) of the flow of

$$\begin{cases} \dot{\mathbf{x}}(t) = -\beta H \mathbf{v}(t), \\ \dot{\mathbf{v}}(t) = -\beta H \mathbf{E}_{[X(t)]}(\mathbf{x}(t)) + \mathbf{v}(t) \times \mathbf{B}(\mathbf{x}(t)). \end{cases} \quad (3.8)$$

The solution at final time T_f is then obtained by applying to $(\mathbf{x}_{\mathbf{v}^M}^M)$ the flow $\mathcal{E}_r(T_r)$ at time T_r of

$$\begin{cases} \dot{\mathbf{x}}(t) = \varepsilon \mathbf{v}(t), \\ \dot{\mathbf{v}}(t) = \varepsilon \mathbf{E}_{[X(t)]}(\mathbf{x}(t)) + \mathbf{v}(t) \times \mathbf{B}(\mathbf{x}(t)). \end{cases} \quad (3.9)$$

Splitting scheme. The full MRC scheme calls for the numerical evaluation of the sub-flows $\mathcal{E}_\alpha(2\pi)$, $\mathcal{E}_\beta(2\pi)$ and $\mathcal{E}_r(T_r)$. This is done here through a splitting, for instance of \mathcal{E}_α , in

$$\mathcal{E}_\alpha^{\mathbf{x}}(t) : \begin{cases} \dot{\mathbf{x}}(s) = \alpha H \mathbf{v}(s), \\ \dot{\mathbf{v}}(s) = 0, \quad 0 < s \leq t, \end{cases} \quad \text{and} \quad \mathcal{E}_\alpha^{\mathbf{v}}(t) : \begin{cases} \dot{\mathbf{x}}(s) = 0, \quad 0 < s \leq t, \\ \dot{\mathbf{v}}(s) = \alpha H \mathbf{E}_{[X(s)]}(\mathbf{x}(s)) + \mathbf{v}(s) \times \mathbf{B}(\mathbf{x}(s)). \end{cases} \quad (3.10)$$

Note that both $\mathcal{E}_\alpha^{\mathbf{x}}(t)$ and $\mathcal{E}_\alpha^{\mathbf{v}}(t)$ can be exactly integrated. The exact flow of $\mathcal{E}_\alpha^{\mathbf{x}}(t)$ is clearly

$$\mathbf{x}(t) = \mathbf{x}(0) + t\alpha H \mathbf{v}(0), \quad \mathbf{v}(t) = \mathbf{v}(0), \quad t \geq 0,$$

while the exact flow of $\mathcal{E}_\alpha^{\mathbf{v}}(t)$, by using the Rodrigues' rotation formula, can also be written explicitly

$$\begin{aligned} \mathbf{x}(t) &= \mathbf{x}(0), \\ \mathbf{v}(t) &= \cos(t)\mathbf{v}(0) + \sin(t)\mathbf{v}(0) \times \mathbf{B} + \alpha H \sin(t)\mathbf{E} + \alpha H(t - \sin(t))(\mathbf{B} \cdot \mathbf{E})\mathbf{B} + \alpha H(1 - \cos(t))\mathbf{E} \times \mathbf{B} \\ &\quad + (1 - \cos(t))(\mathbf{B} \cdot \mathbf{v}(0))\mathbf{B}, \quad t \geq 0, \end{aligned}$$

where $\mathbf{E} = \mathbf{E}_{[X(0)]}(\mathbf{x}(0))$ and $\mathbf{B} = \mathbf{B}(\mathbf{x}(0))$. In our experiments, we shall take the value of the (micro) time step $h = 2\pi/M$, so that

$$\mathcal{E}_\alpha(2\pi) \approx (\mathcal{E}_\alpha^{\mathbf{x}}(h/2)\mathcal{E}_\alpha^{\mathbf{v}}(h)\mathcal{E}_\alpha^{\mathbf{x}}(h/2))^M.$$

Approximations for $\mathcal{E}_\beta(2\pi)$ and $\mathcal{E}_r(T_r)$ are obtained in a similar way. It may then be proved (see (3.6)) that the error of MRC is of size $O(M^{-2})$ for a computational cost of size M^2 , making the overall scheme of order one¹.

It remains to comment on what happens when the user-controlled M increases to the limit where M_0 reaches the critical value $M_0 = 1$, for which $\alpha = 1$, $\beta = 0$ (3.5) and $\mathcal{E}_\beta(-2\pi) \equiv id$. In this case, the full MRC scheme may be regarded as just the discretisation of equation (3.3) by Strang's method with time step h . Therefore, as soon as $M > 0$ implies $M_0 = T_f/\varepsilon/(2\pi)/M < 1$, we replace MRC method by Strang splitting with time step $h = 2\pi/M$. Finally, note that all vector fields involved in MRC are divergence free so that their exact flows are **phase-space volume preserving** as is the MRC method itself.

3.2. Two-scale formulation method. Two-scale formulation (TSF) methods have been developed in [6, 12]. Their underlying rationale is to consider the fast time as an additional variable. In order to isolate the fast time, we apply the change of unknowns $(\mathbf{x}(t), \mathbf{v}(t)) \mapsto (\mathbf{x}(t), \mathbf{y}(t))$ where

$$\mathbf{y}(t) = \cos(t/\varepsilon)\mathbf{v}(t) + (1 - \cos(t/\varepsilon))(\mathbf{B}(\mathbf{x}(t)) \cdot \mathbf{v}(t))\mathbf{B}(\mathbf{x}(t)) - \sin(t/\varepsilon)\mathbf{v}(t) \times \mathbf{B}(\mathbf{x}(t)). \quad (3.11)$$

This leads to

$$\begin{cases} \dot{\mathbf{x}}(t) = F_{\mathbf{x}}(t/\varepsilon, \mathbf{x}(t), \mathbf{y}(t)), \\ \dot{\mathbf{y}}(t) = F_{\mathbf{y}}(t/\varepsilon, \mathbf{x}(t), \mathbf{y}(t)), \quad t > 0, \\ \mathbf{x}(0) = \mathbf{x}_0, \quad \mathbf{y}(0) = \mathbf{v}_0, \end{cases} \quad (3.12)$$

where

$$F_{\mathbf{x}}(\tau, \mathbf{x}, \mathbf{y}) := \cos(\tau)\mathbf{y} + (1 - \cos(\tau))(\mathbf{B}(\mathbf{x}) \cdot \mathbf{y})\mathbf{B}(\mathbf{x}) + \sin(\tau)\mathbf{y} \times \mathbf{B}(\mathbf{x}),$$

¹Under the assumption that $\mathbf{E}(t, \mathbf{x}) \in C^2(\mathbb{R}^+ \times \mathbb{R}^3; \mathbb{R}^3)$ and $\mathbf{B}(\mathbf{x}) \in C^2(\mathbb{R}^3; \mathbb{R}^3)$ in (3.2).

and

$$\begin{aligned}
F_{\mathbf{y}}(\tau, \mathbf{x}, \mathbf{y}) &= \cos(\tau) \mathbf{E}_{[X]}(\mathbf{x}) + (1 - \cos(\tau))(\mathbf{B}(\mathbf{x}) \cdot \mathbf{E}_{[X]}(\mathbf{x}))\mathbf{B}(\mathbf{x}) - \sin(\tau) \mathbf{E}_{[X]}(\mathbf{x}) \times \mathbf{B}(\mathbf{x}) \\
&\quad - \frac{1}{2} \sin(2\tau) \mathbf{q}_{\tau}(\mathbf{y}) - \frac{1}{2} (2 \sin(\tau) - \sin(2\tau)) \mathbf{q}_{\tau}((\mathbf{B}(\mathbf{x}) \cdot \mathbf{y})\mathbf{B}(\mathbf{x})) \\
&\quad - \frac{1}{2} (1 - \cos(2\tau)) \mathbf{q}_{\tau}(\mathbf{y} \times \mathbf{B}(\mathbf{x})) + \frac{1}{2} (2 \cos(\tau) - \cos(2\tau) - 1) \mathbf{p}_{\tau}(\mathbf{y}) + \frac{1}{2} (3 - 4 \cos(\tau) \\
&\quad + \cos(2\tau)) \mathbf{p}_{\tau}((\mathbf{B}(\mathbf{x}) \cdot \mathbf{y})\mathbf{B}(\mathbf{x})) + \frac{1}{2} (2 \sin(\tau) - \sin(2\tau)) \mathbf{p}_{\tau}(\mathbf{y} \times \mathbf{B}(\mathbf{x})),
\end{aligned}$$

with the vector fields

$$\begin{aligned}
\mathbf{p}_{\tau}(\mathbf{z}) &:= ((\nabla_{\mathbf{x}} \mathbf{B}(\mathbf{x}) F_{\mathbf{x}}(\tau, \mathbf{x}, \mathbf{y})) \cdot \mathbf{z}) \mathbf{B}(\mathbf{x}) + (\mathbf{B}(\mathbf{x}) \cdot \mathbf{z}) (\nabla_{\mathbf{x}} \mathbf{B}(\mathbf{x}) F_{\mathbf{x}}(\tau, \mathbf{x}, \mathbf{y})), \\
\mathbf{q}_{\tau}(\mathbf{z}) &:= \mathbf{z} \times (\nabla_{\mathbf{x}} \mathbf{B}(\mathbf{x}) F_{\mathbf{x}}(\tau, \mathbf{x}, \mathbf{y})), \quad \mathbf{z} \in \mathbb{R}^3.
\end{aligned}$$

Denoting $\mathbf{u}(t) = \begin{pmatrix} \mathbf{x}(t) \\ \mathbf{y}(t) \end{pmatrix}$ and $F(\tau, \mathbf{u}) = \begin{pmatrix} F_{\mathbf{x}}(\tau, \mathbf{x}, \mathbf{y}) \\ F_{\mathbf{y}}(\tau, \mathbf{x}, \mathbf{y}) \end{pmatrix}$, the two-scale formulation of system (3.12) now reads

$$\begin{aligned}
\partial_t U(t, \tau) + \frac{1}{\varepsilon} \partial_{\tau} U(t, \tau) &= F(\tau, U(t, \tau)), \quad t > 0, \tau \in \mathbb{T}, \\
U(0, 0) &= \mathbf{u}(0),
\end{aligned} \tag{3.13}$$

where $\mathbb{T} = [0, 2\pi]$, and one recovers the solution of (3.12) by taking the diagonal, i.e.

$$U(t, t/\varepsilon) = \mathbf{u}(t), \quad t \geq 0.$$

It remains to prescribe an appropriate initial data $U(0, \tau)$ to (3.13) so that the solution U has its derivatives uniformly bounded up to some order.

Initial data. In order to derive $U(0, \tau)$, we follow the Chapman-Enskog procedure. From the decomposition

$$\underline{U}(t) = \Pi U(t, \cdot), \quad \mathbf{h}(t, \tau) = U(t, \tau) - \underline{U}(t), \quad \text{with } \Pi U(t, \cdot) = \frac{1}{2\pi} \int_0^{2\pi} U(t, \tau) d\tau,$$

we split (3.13) into

$$\begin{cases} \dot{\underline{U}}(t) = \Pi F(\cdot, \underline{U}(t) + \mathbf{h}(t, \cdot)), & t > 0, \\ \partial_t \mathbf{h}(t, \tau) + \frac{1}{\varepsilon} \partial_{\tau} \mathbf{h}(t, \tau) = (I - \Pi) F(\tau, \underline{U}(t) + \mathbf{h}(t, \tau)), & t > 0, \tau \in \mathbb{T}. \end{cases}$$

Denote $L = \partial_{\tau}$, $A = L^{-1}(I - \Pi)$ and we have

$$\mathbf{h}(t, \tau) = \varepsilon A F(\tau, \underline{U}(t) + \mathbf{h}(t, \tau)) - \varepsilon L^{-1} \partial_t \mathbf{h}(t, \tau).$$

Differentiate the above with respect to t on both sides:

$$\partial_t \mathbf{h}(t, \tau) = \varepsilon A \nabla F(\tau, \underline{U} + \mathbf{h})(\dot{\underline{U}} + \partial_t \mathbf{h}) - \varepsilon L^{-1} \partial_t^2 \mathbf{h}(t, \tau).$$

By assuming that $\partial_t^2 \mathbf{h} = O(1)$ for $\varepsilon \in]0, 1]$, one gets $\partial_t \mathbf{h} = O(\varepsilon)$ and $\mathbf{h}(t, \tau)$ has the first order asymptotic expansion:

$$\mathbf{h}(t, \tau) = \varepsilon A F(\tau, \underline{U}(t)) + O(\varepsilon^2).$$

Using the fact $\underline{U}(0) = \mathbf{u}(0) - \mathbf{h}(0, 0)$, one gets at initial time

$$\mathbf{h}(0, \tau) = \mathbf{h}^{1st}(\tau) + O(\varepsilon^2), \quad \text{with } \mathbf{h}^{1st}(\tau) := \varepsilon A F(\tau, \mathbf{u}(0)),$$

and we denotes the first order initial data as:

$$U^{1st}(\tau) := \mathbf{u}(0) + \mathbf{h}^{1st}(\tau) - \mathbf{h}^{1st}(0). \tag{3.14}$$

In fact, one can show rigorously that the equation (3.13) with the well-prepared initial data $U(0, \tau) = U^{1st}(\tau)$ offers

$$\partial_t U(t, \tau), \partial_t^2 U(t, \tau) = O(1), \quad \varepsilon \in]0, 1]. \tag{3.15}$$

We refer the readers to [6] for the mathematical justification. The boundedness of the time derivatives (3.15) is the key to design UA schemes.

Exponential integrator. Thanks to the two-scale formulation (3.13) with the well-prepared initial data $U(0, \tau) = U^{1st}(\tau)$ from (3.14), we can now directly apply the second order exponential integrator scheme proposed in [15] for integrating (3.13): Choose $N_\tau > 0$ an even integer to uniformly discretize τ on \mathbb{T} and take a $\Delta t > 0$ to define $t_n = n\Delta t$. Denote $U^n(\tau) \approx U(t_n, \tau)$ for $n \geq 0$ and let $U^0(\tau) = U(0, \tau)$. We update the U^n for $n \geq 1$ as

$$\widehat{(U)}_l^1 = e^{-\frac{i l \Delta t}{\varepsilon}} \widehat{(U)}_l^0 + p_l \widehat{(F)}_l^0 + q_l \frac{1}{\Delta t} \left(\widehat{(F)}_l^{*,1} - \widehat{(F)}_l^0 \right), \quad (3.16a)$$

$$\widehat{(U)}_l^{n+1} = e^{-\frac{i l \Delta t}{\varepsilon}} \widehat{(U)}_l^n + p_l \widehat{(F)}_l^n + q_l \frac{1}{\Delta t} \left(\widehat{(F)}_l^n - \widehat{(F)}_l^{n-1} \right), \quad n \geq 1, \quad (3.16b)$$

where for $n \geq 0$,

$$U^n(\tau) = \sum_{l=-N_\tau/2}^{N_\tau/2-1} \widehat{(U)}_l^n e^{il\tau}, \quad F^n(\tau) = \sum_{l=-N_\tau/2}^{N_\tau/2-1} \widehat{(F)}_l^n e^{il\tau}, \quad F^{*,1}(\tau) = \sum_{l=-N_\tau/2}^{N_\tau/2-1} \widehat{(F)}_l^{*,1} e^{il\tau},$$

and $F^n(\tau) = F(\tau, U^n(\tau))$, $F^{*,1}(\tau) = F(\tau, U^{*,1}(\tau))$ with

$$\widehat{(U)}_l^{*,1} = e^{-\frac{i l \Delta t}{\varepsilon}} \widehat{(U)}_l^0 + p_l \widehat{(F)}_l^0, \quad U^{*,1}(\tau) = \sum_{l=-N_\tau/2}^{N_\tau/2-1} \widehat{(U)}_l^{*,1} e^{il\tau},$$

and

$$p_l = \begin{cases} \frac{i\varepsilon}{l} \left(e^{-\frac{i l \Delta t}{\varepsilon}} - 1 \right), & l \neq 0, \\ \Delta t, & l = 0, \end{cases} \quad q_l = \begin{cases} \frac{\varepsilon}{l^2} \left(\varepsilon - \varepsilon e^{-\frac{i l \Delta t}{\varepsilon}} - i l \Delta t \right), & l \neq 0, \\ \frac{\Delta t^2}{2}, & l = 0. \end{cases}$$

Suppose we have the numerical solution $U^n(\tau) = \begin{pmatrix} X^n(\tau) \\ Y^n(\tau) \end{pmatrix}$ from the above scheme, then the numerical solution $\mathbf{x}^n \approx \mathbf{x}(t_n)$, $\mathbf{v}^n \approx \mathbf{v}(t_n)$ of the original characteristics (3.2) reads:

$$\mathbf{x}^n = X^n(t_n/\varepsilon), \quad n \geq 1,$$

$$\mathbf{v}^n = \cos(t_n/\varepsilon) Y^n(t_n/\varepsilon) + (1 - \cos(t_n/\varepsilon)) (\mathbf{B}(\mathbf{x}^n) \cdot Y^n(t_n/\varepsilon)) \mathbf{B}(\mathbf{x}^n) + \sin(t_n/\varepsilon) Y^n(t_n/\varepsilon) \times \mathbf{B}(\mathbf{x}^n).$$

The derivation and convergence analysis of the above scheme can be found in [15]. Since the filter (3.11) involves the magnetic field $\mathbf{B}(\mathbf{x})$, the filtered system (3.12) which is less smooth than the original form (3.2), needs more regularity for optimal convergence of the algorithm. Assuming that $\mathbf{E}(t, \mathbf{x}) \in C^2(\mathbb{R}^+ \times \mathbb{R}^3; \mathbb{R}^3)$ and $\mathbf{B}(\mathbf{x}) \in C^3(\mathbb{R}^3; \mathbb{R}^3)$ in (3.2), the two-scale formulation (TSF) exponential integrator (3.16) gives uniform second order accuracy in terms of Δt for all $\varepsilon \in]0, 1]$ and uniform spectral accuracy in terms of N_τ (due to periodicity):

$$O(\Delta t^2 + N_\tau^{-m_0}).$$

The total cost of the TSF method is $O(\Delta t^{-1} N_\tau \log N_\tau)$.

3.3. Micro-macro method. Now, we present the main new method of this work. It is based on the micro-macro (MM) decomposition that has been proposed very recently in [7]. We shall for the first time consider this approach for the Vlasov-Poisson equation and propose a second order UA scheme. The same notations will be adopted from the previous subsection.

MM decomposition. By the averaging theory [34], it is known that for general oscillatory problem

$$\dot{\mathbf{u}}(t) = F(t/\varepsilon, \mathbf{u}(t)), \quad t > 0, \quad (3.17)$$

with 2π -periodicity in τ of $F(\tau, \mathbf{u})$, the solution can be written as a composition

$$\mathbf{u}(t) = \Phi_{t/\varepsilon} \circ \Psi_t \circ \Phi_0^{-1}(\mathbf{u}(0)), \quad (3.18)$$

where $\Phi_\tau(\mathbf{v})$ is a change of variable with 2π -periodicity in τ for some \mathbf{v} , and $\Psi_t(\mathbf{v})$ is the flow map of the autonomous equation with initial value \mathbf{v} :

$$\dot{\Psi}_t(\mathbf{v}) = F_0(\Psi_t(\mathbf{v})), \quad \Psi_0(\mathbf{v}) = \mathbf{v},$$

for some field F_0 . Though (3.18) is known to hold theoretically for some Φ_τ and Ψ_t , the explicit formulas of Φ_τ and Ψ_t are not available. In fact, by plugging (3.18) back to the equation (3.17), the change of variable Φ_τ , the flow map Ψ_t and the averaged field F_0 can be seen to satisfy the relation

$$\frac{1}{\varepsilon} \partial_\tau \Phi_\tau(\mathbf{v}) + D_{\mathbf{v}} \Phi_\tau(\mathbf{v}) F_0(\mathbf{v}) = F(\tau, \Phi_\tau(\mathbf{v})), \quad (3.19)$$

and moreover by taking averaging with respect to $\tau \in [0, 2\pi]$ on both sides of (3.19), one can define F_0 with Φ_τ ,

$$F_0 = (\Pi D_{\mathbf{v}} \Phi_\tau)^{-1} \Pi F(\cdot, \Phi_\tau).$$

The above two equalities cannot completely determine Φ_τ and Ψ_t , so the standard averaging method imposes an extra condition $\Pi \Phi_\tau = id$, which uniquely defines the change of variable Φ_τ in an implicit way through (3.19). In general, it is not possible to solve (3.19) to find out the exact Φ_τ . However, we can define an approximated Φ_τ through a k th-order iteration

$$\Phi_\tau^{[k+1]} = id + \varepsilon A \left(F(\tau, \Phi_\tau^{[k]}) - D_{\mathbf{v}} \Phi_\tau^{[k]} F_0^{[k]} \right), \quad k \in \mathbb{N}, \quad (3.20)$$

with initially

$$\Phi_\tau^{[0]} = id, \quad F_0^{[0]} = \Pi F,$$

which asymptotically gives

$$\Phi_\tau = \Phi_\tau^{[k]} + O(\varepsilon^{k+1}).$$

As a compensation to the composition (3.18) by using the approximated function $\Phi_\tau^{[k]}$, a defect $\mathbf{w}^{[k]}$ needs to be introduced:

$$\mathbf{u}(t) = \Phi_{t/\varepsilon}^{[k]} \circ \Psi_t^{[k]} \circ (\Phi_0^{[k]})^{-1}(\mathbf{u}(0)) + \mathbf{w}^{[k]}(t), \quad (3.21)$$

to ensure that there are no asymptotical truncations made to the exact solution. The decomposition (3.21) is referred as the micro-macro decomposition of the solution of (3.17).

As a matter of fact, the first order approximation $\Phi_\tau^{[1]}$ given by the micro-macro decomposition, i.e. $k = 0$ in (3.20), coincides with the first order Chapman-Enskog expansion that we introduced in the previous subsection:

$$\Phi_\tau^{[1]}(\mathbf{r}) = \mathbf{r} + \varepsilon A F(\tau, \mathbf{r}) =: \Theta(\tau, \mathbf{r}).$$

Thus, (3.12) or (3.17) has the first order micro-macro decomposition:

$$\mathbf{u}(t) = \Theta(t/\varepsilon, \mathbf{r}(t)) + \mathbf{w}(t), \quad t \geq 0, \quad (3.22)$$

where the macro part representing the averaged equation reads

$$\begin{cases} \dot{\mathbf{r}}(t) = \Pi F(\cdot, \Theta(\cdot, \mathbf{r}(t))), & t > 0, \\ \mathbf{r}(0) = \mathbf{u}(0) - \varepsilon A F(\tau, \mathbf{u}(0))|_{\tau=0}, \end{cases} \quad (3.23)$$

and the micro part representing the equation for the defect reads

$$\begin{cases} \dot{\mathbf{w}}(t) = G(t/\varepsilon, \mathbf{r}(t), \mathbf{w}(t)), & t > 0, \\ \mathbf{w}(0) = \varepsilon A [F(\tau, \mathbf{u}(0)) - F(\tau, \mathbf{r}(0))] |_{\tau=0}, \end{cases} \quad (3.24)$$

with

$$G(\tau, \mathbf{r}, \mathbf{w}) := F(\tau, \Theta(\tau, \mathbf{r}) + \mathbf{w}) - (I - \Pi)F(\tau, \mathbf{r}) - \frac{d}{dt} \Theta(\tau, \mathbf{r}(t)).$$

In the first order micro-macro decomposition, the macro part (3.23) is smooth containing no high-frequencies. As for the micro part, it can be shown that [7]

$$\mathbf{w}(t) = O(\varepsilon^2), \quad \partial_t \mathbf{w}(t) = O(\varepsilon), \quad \partial_t^2 \mathbf{w}(t) = O(1).$$

Thanks to the reformulation (3.12), we are able to consider this micro-macro approach for the characteristics (3.2).

An integration scheme. Now based on the micro-macro decomposed systems (3.23) and (3.24), we are going to propose a second order integration for solving (3.17) which is a compact formulation

of (3.12) with $\mathbf{u}(t) = \begin{pmatrix} \mathbf{x}(t) \\ \mathbf{y}(t) \end{pmatrix}$ and $F(\tau, \mathbf{u}) = \begin{pmatrix} F_{\mathbf{x}}(\tau, \mathbf{x}, \mathbf{y}) \\ F_{\mathbf{y}}(\tau, \mathbf{x}, \mathbf{y}) \end{pmatrix}$. We solve the macro part (3.23) by a leap-frog finite difference scheme:

$$\mathbf{r}^{n+1} = \mathbf{r}^{n-1} + 2\Delta t \Pi F(\cdot, \Theta(\cdot, \mathbf{r}^n)), \quad n \geq 1, \quad \mathbf{r}^1 = \mathbf{r}^0 + \Delta t \Pi F(\cdot, \Theta(\cdot, \mathbf{r}^0)).$$

For the micro part (3.24), we integrate the equation to have

$$\begin{aligned} \mathbf{w}(t_{n+1}) - \mathbf{w}(t_n) &= \int_{t_n}^{t_{n+1}} G(t/\varepsilon, \mathbf{r}(t), \mathbf{w}(t)) dt \\ &= \int_{t_n}^{t_{n+1}} H(t/\varepsilon, \mathbf{r}(t), \mathbf{w}(t)) dt - \Theta(t_{n+1}/\varepsilon, \mathbf{r}(t_{n+1})) + \Theta(t_n/\varepsilon, \mathbf{r}(t_n)), \end{aligned} \quad (3.25)$$

where

$$H(\tau, \mathbf{r}, \mathbf{w}) := F(\tau, \Theta(\tau, \mathbf{r}) + \mathbf{w}).$$

Since $H(\tau, \mathbf{r}, \mathbf{w})$ is periodic in $\tau \in \mathbb{T}$, so we have a Fourier expansion

$$H(\tau, \mathbf{r}, \mathbf{w}) = \sum_{l \in \mathbb{Z}} \widehat{H}_l(\mathbf{r}, \mathbf{w}) e^{il\tau},$$

and the integration in (3.25) can be approximated as

$$\begin{aligned} \int_{t_n}^{t_{n+1}} H(t/\varepsilon, \mathbf{r}(t), \mathbf{w}(t)) dt &= \sum_{l \in \mathbb{Z}} \int_{t_n}^{t_{n+1}} \widehat{H}_l(\mathbf{r}(t), \mathbf{w}(t)) e^{ilt/\varepsilon} dt \\ &\approx \sum_{l \in \mathbb{Z}} \int_{t_n}^{t_{n+1}} \left[\widehat{H}_l(\mathbf{r}(t_n), \mathbf{w}(t_n)) + (t - t_n) \frac{d}{dt} \widehat{H}_l(\mathbf{r}(t_n), \mathbf{w}(t_n)) \right] e^{ilt/\varepsilon} dt \\ &\approx \sum_{l \in \mathbb{Z}} \int_{t_n}^{t_{n+1}} \left[\widehat{H}_l(\mathbf{r}(t_n), \mathbf{w}(t_n)) + \frac{t - t_n}{\Delta t} \left(\widehat{H}_l(\mathbf{r}(t_n), \mathbf{w}(t_n)) - \widehat{H}_l(\mathbf{r}(t_{n-1}), \mathbf{w}(t_{n-1})) \right) \right] e^{ilt/\varepsilon} dt. \end{aligned}$$

Therefore, for $n \geq 1$,

$$\begin{aligned} \mathbf{w}(t_{n+1}) &\approx \mathbf{w}(t_n) + \sum_{l \in \mathbb{Z}} e^{ilt_n/\varepsilon} \left[\alpha_l \widehat{H}_l(\mathbf{r}(t_n), \mathbf{w}(t_n)) + \frac{\beta_l}{\Delta t} \left(\widehat{H}_l(\mathbf{r}(t_n), \mathbf{w}(t_n)) - \widehat{H}_l(\mathbf{r}(t_{n-1}), \mathbf{w}(t_{n-1})) \right) \right] \\ &\quad - \Theta(t_{n+1}/\varepsilon, \mathbf{r}(t_{n+1})) + \Theta(t_n/\varepsilon, \mathbf{r}(t_n)), \end{aligned}$$

and as for $n = 0$,

$$\mathbf{w}(t_1) \approx \mathbf{w}(0) + \sum_{l \in \mathbb{Z}} \alpha_l \widehat{H}_l(\mathbf{r}(0), \mathbf{w}(0)) - \Theta(t_1/\varepsilon, \mathbf{r}(t_1)) + \Theta(0, \mathbf{r}(0)),$$

where

$$\begin{aligned} \alpha_l &= \int_0^{\Delta t} e^{ilt/\varepsilon} dt = \begin{cases} \frac{i\varepsilon}{l} \left(1 - e^{\frac{il\Delta t}{\varepsilon}} \right), & l \neq 0, \\ \Delta t, & l = 0, \end{cases} \\ \beta_l &= \int_0^{\Delta t} t e^{ilt/\varepsilon} dt = \begin{cases} \frac{\varepsilon}{l^2} \left((\varepsilon - il\Delta t) e^{\frac{il\Delta t}{\varepsilon}} - \varepsilon \right), & l \neq 0, \\ \frac{\Delta t^2}{2}, & l = 0. \end{cases} \end{aligned}$$

In total, the detailed exponential integration scheme based on the micro-macro method reads:

$$\mathbf{u}^{n+1} = \Theta(t_{n+1}/\varepsilon, \mathbf{r}^{n+1}) + \mathbf{w}^{n+1}, \quad n \geq 0, \quad (3.26a)$$

$$\mathbf{r}^{n+1} = \mathbf{r}^{n-1} + 2\Delta t \Pi F(\cdot, \Theta(\cdot, \mathbf{r}^n)), \quad n \geq 1, \quad (3.26b)$$

$$\begin{aligned} \mathbf{w}^{n+1} = & \mathbf{w}^n + \sum_{l=-N_\tau/2}^{N_\tau/2-1} e^{i l t_n / \varepsilon} \left[\alpha_l \widehat{H}_l(\mathbf{r}^n, \mathbf{w}^n) + \frac{\beta_l}{\Delta t} \left(\widehat{H}_l(\mathbf{r}^n, \mathbf{w}^n) - \widehat{H}_l(\mathbf{r}^{n-1}, \mathbf{w}^{n-1}) \right) \right] \\ & - \Theta(t_{n+1}/\varepsilon, \mathbf{r}^{n+1}) + \Theta(t_n/\varepsilon, \mathbf{r}^n), \quad n \geq 1, \end{aligned} \quad (3.26c)$$

$$\mathbf{r}^1 = \mathbf{r}^0 + \Delta t \Pi F(\cdot, \Theta(\cdot, \mathbf{r}^0)), \quad \mathbf{w}^1 = \mathbf{w}^0 + \sum_{l=-N_\tau/2}^{N_\tau/2-1} \alpha_l \widehat{H}_l(\mathbf{r}^0, \mathbf{w}^0) - \Theta(t_1/\varepsilon, \mathbf{r}^1) + \Theta(0, \mathbf{r}^0), \quad (3.26d)$$

$$\mathbf{r}^0 = \mathbf{u}(0) - \varepsilon A F(\tau, \mathbf{u}(0))|_{\tau=0}, \quad \mathbf{w}^0 = \varepsilon A [F(\tau, \mathbf{u}(0)) - F(\tau, \mathbf{r}(0))] |_{\tau=0}, \quad (3.26e)$$

where N_τ is an even integer to truncate the Fourier series. Suppose the numerical solution of MM is obtained as $\mathbf{u}^n = (\mathbf{x}_n^n)$, then the numerical velocity of (3.2) at t_n is given as

$$\mathbf{v}^n = \cos(t_n/\varepsilon) \mathbf{y}^n + (1 - \cos(t_n/\varepsilon)) (\mathbf{B}(\mathbf{x}^n) \cdot \mathbf{y}^n) \mathbf{B}(\mathbf{x}^n) + \sin(t_n/\varepsilon) \mathbf{y}^n \times \mathbf{B}(\mathbf{x}^n).$$

The micro-macro (MM) scheme (3.26) is uniformly second order accurate. In practical programming, one only needs a subroutine to evaluate $F(\tau, \mathbf{u})$. When the electric and magnetic field \mathbf{E} and \mathbf{B} in particle system (3.2) are given external functions such as polynomials, the dependence of the fast time scale t/ε (or τ) in F and Θ can be found out explicitly and the averaging with respect to τ (through the operator Π) in the MM scheme can be pre-computed exactly. Then the MM method will have a discretisation error in time of $O(\Delta t^2)$ with optimal computational cost $O(\Delta t^{-1})$. In case that the exact evaluation of t/ε is impossible or too costly, one can always perform those computations of the fast time scale with the additional variable τ by FFT with uniform spectral accuracy thanks to the periodicity. In such case, the error bound of MM is

$$O(\Delta t^2 + N_\tau^{-m_0}),$$

and the total cost is $O(\Delta t^{-1} N_\tau \log N_\tau)$, which are the same as TSF.

Full recovery of oscillation. Since MM method finds out the dependence of the fast scale in a rather explicit way, it can easily recover the complete gyro-motion of the particles, i.e. the full oscillatory trajectory of the solution of (3.2), by interpolating respectively the macro part and micro part.

Let \mathbf{r}^n and \mathbf{w}^n be the numerical solutions obtained from MM under a step size $\Delta t > 0$. For an arbitrary $t > 0$, if $t_n < t < t_{n+1}$, then we can use the linear interpolation to get

$$\mathbf{r}_I^n(t) = \frac{t_{n+1} - t}{\Delta t} \mathbf{r}^n + \frac{t - t_n}{\Delta t} \mathbf{r}^{n+1}, \quad \mathbf{w}_I^n(t) = \frac{t_{n+1} - t}{\Delta t} \mathbf{w}^n + \frac{t - t_n}{\Delta t} \mathbf{w}^{n+1}.$$

Noting that $\mathbf{r}(t)$ is the averaged part and $\mathbf{w}(t)$ satisfies $\partial_t^2 \mathbf{w}(t) = O(1)$, together with the accuracy order of \mathbf{r}^n and \mathbf{w}^n from the MM scheme, it is clear that the above linear interpolation gives uniform second accuracy for approximating $\mathbf{r}(t)$ and $\mathbf{w}(t)$. Then with micro-macro decomposition (3.22), we get the interpolated numerical solution of (3.17) as

$$\mathbf{u}_I^n(t) = \Theta(t/\varepsilon, \mathbf{r}_I^n(t)) + \mathbf{w}_I^n(t), \quad t_n \leq t \leq t_{n+1}, \quad (3.27)$$

which fully recovers the oscillation information with ease. It is direct to see

$$|\mathbf{u}(t) - \mathbf{u}_I^n(t)| = O(\Delta t^2 + N_\tau^{-m_0}).$$

Restart strategy. In practical long time computing, we observe that the MM scheme (3.26) could have numerical instability issue. The instability is developed from the micro part (3.24) in MM decomposition (3.22) as time evolves, since $\mathbf{w}(t) = O(\varepsilon)$ does not hold for arbitrary long time in general. Here, we propose a restart strategy to improve its long time performance.

Choose $T_0 > 0$ as the period to restart the MM decomposition. For some $m \in \mathbb{N}$, we consider the oscillatory problem (3.17) for $\mathbf{u}^m(t) = \mathbf{u}(mT_0 + t)$ as

$$\dot{\mathbf{u}}^m(t) = F(mT_0/\varepsilon + t/\varepsilon, \mathbf{u}^m(t)), \quad 0 < t \leq T_0.$$

Then we apply the proposed MM strategy on the above, which leads to MM decomposition as

$$\mathbf{u}^m(t) = \Theta(mT_0/\varepsilon + t/\varepsilon, \mathbf{r}(t)) + \mathbf{w}(t), \quad 0 \leq t \leq T_0, \quad (3.28)$$

with

$$\begin{cases} \dot{\mathbf{r}}(t) = \Pi F(mT_0/\varepsilon + \cdot, \Theta(mT_0/\varepsilon + \cdot, \mathbf{r}(t))), & 0 < t \leq T_0, \\ \mathbf{r}(0) = \mathbf{u}^m(0) - \varepsilon A F(mT_0/\varepsilon + \tau, \mathbf{u}^m(0))|_{\tau=0}, \end{cases}$$

and

$$\begin{cases} \dot{\mathbf{w}}(t) = G(mT_0/\varepsilon + t/\varepsilon, \mathbf{r}(t), \mathbf{w}(t)), & 0 < t \leq T_0, \\ \mathbf{w}(0) = \varepsilon A [F(mT_0/\varepsilon + \tau, \mathbf{u}^m(0)) - F(mT_0/\varepsilon + \tau, \mathbf{r}(0))] |_{\tau=0}. \end{cases}$$

The integration scheme (3.26) is then applied to solve the above two systems.

As can be seen in the numerical results later, this restart strategy for solving (3.2) is stable in long time computing. Its accuracy and computational cost are essentially the same as the direct scheme without restart.

Remark 3.1. In the case that $\mathbf{B}(\mathbf{x}) = \mathbf{B}_0(\mathbf{x}) + O(\varepsilon)$ with $|\mathbf{B}_0(\mathbf{x})| \equiv \text{const}$, all the proposed algorithms in this section can be extended to such case without any essential difficulties.

Remark 3.2. Although physically the magnetic field should be divergence free, i.e. $\nabla_{\mathbf{x}} \cdot \mathbf{B} = 0$, all the algorithms we proposed in this section do not rely on the divergence free property of $\mathbf{B}(\mathbf{x})$ to offer the uniform accuracy.

4. EXTENSION TO VARYING INTENSITY MAGNETIC FIELD

In this section, we extend previous methods to the case of Vlasov equation with a general magnetic field (whose intensity may vary), i.e.

$$|\mathbf{B}(\mathbf{x})| = b(\mathbf{x}) \neq \text{const}, \quad \mathbf{x} \in \mathbb{R}^3.$$

We start by commenting on the difficulties to be encountered in this situation. As soon as $|\mathbf{B}(\mathbf{x})| = b(\mathbf{x})$ varies with \mathbf{x} while remaining bounded from below by some c_0 independent of ε , the characteristic equation for each particle

$$\begin{aligned} \dot{\mathbf{x}}_k(t) &= \mathbf{v}_k(t), \\ \dot{\mathbf{v}}_k(t) &= \mathbf{E}(t, \mathbf{x}_k(t)) + \frac{1}{\varepsilon} \mathbf{v}_k(t) \times \mathbf{B}(\mathbf{x}_k(t)), \quad t > 0, \end{aligned}$$

generate high oscillations. However, the dynamics of the linear part of the equation is non-periodic and thus does not allow for the application of averaging techniques. A possible remedy consists in time-reparametrisation. However, another difficulty then arises from the Poisson equation itself

$$\nabla_{\mathbf{x}} \cdot \mathbf{E}(t, \mathbf{x}) = \sum_{k=1}^{N_p} w_k \delta(\mathbf{x} - \mathbf{x}_k(t)),$$

which couples a huge number ($N_p \gg 1$) of particles with different frequencies.

Rescaling the time for each particle. Each particle has a periodic oscillation with respect to its own time $s_k = s_k(t)$, given by

$$\dot{s}_k(t) = b(\mathbf{x}_k(t)), \quad s_k(0) = 0. \quad (4.1)$$

Note that $s_k(t)$ is strictly increasing and that

$$s_k(t) \rightarrow \infty, \quad \text{as } t \rightarrow \infty,$$

since $b(\mathbf{x}) \geq c_0 > 0$. Denoting $\tilde{\mathbf{x}}_k(s_k) := \mathbf{x}_k(t)$, $\tilde{\mathbf{v}}_k(s_k) := \mathbf{v}_k(t)$, we indeed have

$$\begin{cases} \frac{d}{ds_k} \tilde{\mathbf{x}}_k(s_k) = \frac{\tilde{\mathbf{v}}_k(s_k)}{b(\tilde{\mathbf{x}}_k(s_k))}, \\ \frac{d}{ds_k} \tilde{\mathbf{v}}_k(s_k) = \frac{\mathbf{E}(t(s_k), \tilde{\mathbf{x}}_k(s_k))}{b(\tilde{\mathbf{x}}_k(s_k))} + \frac{1}{\varepsilon} \tilde{\mathbf{v}}_k(s_k) \times \frac{\mathbf{B}(\tilde{\mathbf{x}}_k(s_k))}{b(\tilde{\mathbf{x}}_k(s_k))}, & s_k > 0, \\ \tilde{\mathbf{x}}_k(0) = \mathbf{x}_{k,0}, \quad \tilde{\mathbf{v}}_k(0) = \mathbf{v}_{k,0}, \end{cases} \quad (4.2)$$

where the intensity of the magnetic field is scaled to one. Assuming that the electric field $\mathbf{E}(t, \mathbf{x})$ is a given external field with no ε -dependent oscillation in t , then the particle system (4.2) is decoupled for each k . Therefore, the numerical methods introduced in the previous section can all be applied to (4.2) for each particle in its own time s_k with uniform accuracy.

In order to build up an approximation of the function $f^\varepsilon(t, \mathbf{x}, \mathbf{v})$ through (3.1), it is then necessary to re-synchronise for all particles. However, reverting s_k to the physical time t is not straightforward, as it requires to numerically solve the nonlinear equation (4.1) or its equivalent for the inverse map

$$\dot{t}(s_k) = 1/b(\tilde{\mathbf{x}}_k(s_k)), \quad t(0) = 0. \quad (4.3)$$

Given a physical time $t = T > 0$ (or conversely $S_k > 0$), the best we can hope for is to determine $s_k(T)$ (or conversely $t(S_k)$) up to an error of size $O(\Delta t^p)$ if a p th-order numerical method is applied. This source of possible error needs to be properly controlled. Here we illustrate how it can be done for the micro-macro (MM) method.

Interpolating to synchronise. For the sake of brevity, we omit k and denote

$$\tilde{\mathbf{B}}(\tilde{\mathbf{x}}) = \frac{\mathbf{B}(\tilde{\mathbf{x}})}{b(\tilde{\mathbf{x}})}, \quad \tilde{\mathbf{E}}(t, \tilde{\mathbf{x}}) = \frac{\mathbf{E}(t, \tilde{\mathbf{x}})}{b(\tilde{\mathbf{x}})}.$$

We filter (4.2) and (4.3) as before by introducing

$$\tilde{\mathbf{y}}(s) := \cos(s/\varepsilon)\tilde{\mathbf{v}}(s) + (1 - \cos(s/\varepsilon))(\tilde{\mathbf{B}}(\tilde{\mathbf{x}}(s)) \cdot \tilde{\mathbf{v}}(s))\tilde{\mathbf{B}}(\tilde{\mathbf{x}}(s)) - \sin(s/\varepsilon)\tilde{\mathbf{v}}(s) \times \tilde{\mathbf{B}}(\tilde{\mathbf{x}}(s)), \quad (4.4)$$

and obtain

$$\begin{cases} \frac{d}{ds} \tilde{\mathbf{x}}(s) = \tilde{F}_{\mathbf{x}}(s/\varepsilon, \tilde{\mathbf{x}}(s), \tilde{\mathbf{y}}(s)), \\ \frac{d}{ds} \tilde{\mathbf{y}}(s) = \tilde{F}_{\mathbf{y}}(s/\varepsilon, \tilde{\mathbf{x}}(s), \tilde{\mathbf{y}}(s)), & s > 0, \\ \frac{d}{ds} t(s) = \frac{1}{b(\tilde{\mathbf{x}}(s))}, \\ \tilde{\mathbf{x}}(0) = \mathbf{x}_0, \quad \tilde{\mathbf{y}}(0) = \mathbf{v}_0, \quad t(0) = 0, \end{cases} \quad (4.5)$$

which has now the appropriate format (3.17). Here $\tilde{F}_{\mathbf{y}}$ is defined similarly as in (3.12) (see Section 3.2) with the scaled vector fields $\tilde{\mathbf{E}}$, $\tilde{\mathbf{B}}$ and $\tilde{F}_{\mathbf{x}} = F_{\mathbf{x}}/b(\tilde{\mathbf{x}})$. We then solve system (4.5) with the MM scheme (3.26) with time step $\Delta s > 0$ and denote $t^n \approx t(s_n)$ the numerical solution of $t(s_n)$ at $s_n = n\Delta s$. Then, using the notations $\mathbf{r} := (\mathbf{r}_{\mathbf{x}}, \mathbf{r}_{\mathbf{y}})$ and $\mathbf{w} = (\mathbf{w}_{\mathbf{x}}, \mathbf{w}_{\mathbf{y}})$ for the macro and micro parts (see Section 3.3), the numerical solution of $\tilde{\mathbf{x}}$ and $\tilde{\mathbf{y}}$ at $s_n = n\Delta s$ is

$$\tilde{\mathbf{x}}^n := \mathbf{r}_{\mathbf{x}}^n + \varepsilon A \tilde{F}_{\mathbf{x}}(s_n/\varepsilon, \mathbf{r}_{\mathbf{x}}^n, \mathbf{r}_{\mathbf{y}}^n) + \mathbf{w}_{\mathbf{x}}^n \approx \tilde{\mathbf{x}}(s_n), \quad \tilde{\mathbf{y}}^n := \mathbf{r}_{\mathbf{y}}^n + \varepsilon A \tilde{F}_{\mathbf{y}}(s_n/\varepsilon, \mathbf{r}_{\mathbf{x}}^n, \mathbf{r}_{\mathbf{y}}^n) + \mathbf{w}_{\mathbf{y}}^n \approx \tilde{\mathbf{y}}(s_n).$$

Assume that $b(\cdot) \in C^1(\mathbb{R}^3)$ and $0 < c_0 \leq b(\mathbf{x}) \leq C_b$ for all $\mathbf{x} \in \mathbb{R}^3$ for some $C_b > 0$. Then, from

$$t^n \geq t(s_n) - |t^n - t(s_n)| \geq \frac{s_n}{C_b} - C\Delta s^2$$

we see that whenever $\Delta s > 0$ is small enough, the value of t^n will eventually become greater than any arbitrary positive value. For a given final time $T > 0$, we thus stop the algorithm when $t^n \leq T \leq t^{n+1}$. Note that the function $t(s)$ satisfies

$$\frac{d^2}{ds^2} t(s) = O(1), \quad 0 < \varepsilon \leq 1,$$

so that we can interpolate the value of $t(s)$ from t^n and t^{n+1} with second order uniform accuracy:

$$\theta := \frac{T - t^{n+1}}{t^n - t^{n+1}}, \quad T = \theta t^n + (1 - \theta)t^{n+1}, \quad s^* = \theta s^n + (1 - \theta)s^{n+1}.$$

Interpolation is further used to obtain

$$\begin{aligned} \mathbf{r}_x^* &= \theta \mathbf{r}_x^n + (1 - \theta) \mathbf{r}_x^{n+1}, & \mathbf{r}_y^* &= \theta \mathbf{r}_y^n + (1 - \theta) \mathbf{r}_y^{n+1}, \\ \mathbf{w}_x^* &= \theta \mathbf{w}_x^n + (1 - \theta) \mathbf{w}_x^{n+1}, & \mathbf{w}_y^* &= \theta \mathbf{w}_y^n + (1 - \theta) \mathbf{w}_y^{n+1}. \end{aligned}$$

As stated in Section 3.3, all functions used above in the interpolation have uniformly bounded second order derivative. As a consequence, the so-obtained approximations are uniformly second order. Eventually, the numerical solutions of (4.5) at $s = s(T)$ are given by

$$\tilde{\mathbf{x}}(s(T)) \approx \tilde{\mathbf{x}}^*, \quad \tilde{\mathbf{y}}(s(T)) \approx \tilde{\mathbf{y}}^*,$$

with

$$\tilde{\mathbf{x}}^* := \mathbf{r}_x^* + \varepsilon A \tilde{F}_x(s^*/\varepsilon, \mathbf{r}_x^*, \mathbf{r}_y^*) + \mathbf{w}_x^*, \quad \tilde{\mathbf{y}}^* := \mathbf{r}_y^* + \varepsilon A \tilde{F}_y(s^*/\varepsilon, \mathbf{r}_x^*, \mathbf{r}_y^*) + \mathbf{w}_y^*. \quad (4.6)$$

Note that the dependence in the fast-time s/ε within the MM method only appears in the $O(\varepsilon)$ -terms. As a consequence, the approximation errors of $\tilde{\mathbf{x}}(s(T))$ and $\tilde{\mathbf{y}}(s(T))$ by (4.6) are still of uniform second order, although an error is introduced on s^*/ε owing to $|s(T) - s^*|/\varepsilon = O(\Delta s^2/\varepsilon)$.

To reconstruct an approximation of the distribution function $f^\varepsilon(T, \mathbf{x}, \mathbf{v})$, we need $\mathbf{x}(T)$ and $\mathbf{v}(T)$. For the position variable, we directly have $\mathbf{x}(T) = \tilde{\mathbf{x}}(s(T))$ due to the definition. As for the velocity variable $\mathbf{v}(T)$, we need to invert the change of variable (4.4), where the fast scale s/ε occurs in some $O(1)$ -terms. However, the parallel component $\mathbf{v}_\parallel := (\mathbf{B} \cdot \mathbf{v})\mathbf{B}/\|\mathbf{B}\|^2$ of the velocity as well as $|\mathbf{v}|$ do not suffer from the same problem, thanks to the following observations (let us recall that $\|\tilde{\mathbf{B}}(\tilde{\mathbf{x}}(s))\|^2 = 1$)

$$\tilde{\mathbf{v}}_\parallel(s) = (\tilde{\mathbf{B}}(\tilde{\mathbf{x}}(s)) \cdot \tilde{\mathbf{y}}(s)) \tilde{\mathbf{B}}(\tilde{\mathbf{x}}(s)), \quad |\tilde{\mathbf{v}}(s)| = |\tilde{\mathbf{y}}(s)|,$$

which allow to get

$$\mathbf{v}_\parallel(T) \approx (\tilde{\mathbf{B}}(\tilde{\mathbf{x}}(s(T))) \cdot \tilde{\mathbf{y}}(s(T))) \tilde{\mathbf{B}}(\tilde{\mathbf{x}}(s(T))), \quad |\mathbf{v}(T)| = |\tilde{\mathbf{y}}(s(T))|.$$

Therefore, the strategy proposed in this section is of overall uniform second order for the computation of

$$\mathbf{x}(t), \quad \mathbf{v}_\parallel(t), \quad |\mathbf{v}(t)|, \quad t \geq 0.$$

This, in turn, allows for a uniformly accurate approximation of macroscopic quantities such as the density or the kinetic energy

$$\rho^\varepsilon(t, \mathbf{x}) := \int_{\mathbb{R}^3} f^\varepsilon(t, \mathbf{x}, \mathbf{v}) d\mathbf{v}, \quad \rho_\mathbf{v}^\varepsilon(t, \mathbf{x}) := \int_{\mathbb{R}^3} |\mathbf{v}|^2 f^\varepsilon(t, \mathbf{x}, \mathbf{v}) d\mathbf{v},$$

as well as the magnetic moment [25, 31]

$$\mu^\varepsilon(t) := \int_{\mathbb{R}^3} \int_{\mathbb{R}^3} f^\varepsilon(t, \mathbf{x}, \mathbf{v}) \frac{|\mathbf{v}_\perp|^2}{|\mathbf{B}(\mathbf{x})|} d\mathbf{x} d\mathbf{v}, \quad (4.7)$$

with $\mathbf{v}_\perp := \mathbf{v} - \mathbf{v}_\parallel$.

5. NUMERICAL RESULTS

This section is devoted to present the numerical results from the proposed numerical schemes. We shall firstly test and compare the accuracy, efficiency and long time performance of the schemes considering a single test particle for some three dimensional simulations in the two following cases: constant intensity and varying intensity magnetic field. Then, we shall focus on the nonlinear Vlasov-Poisson case under the influence of a constant intensity magnetic field.

5.1. Accuracy study. We investigate the performance of the proposed numerical methods by considering a single particle system in three dimensions:

$$\begin{aligned}\dot{\mathbf{x}}(t) &= \mathbf{v}(t), \\ \dot{\mathbf{v}}(t) &= \mathbf{E}(\mathbf{x}(t)) + \frac{1}{\varepsilon} \mathbf{v}(t) \times \mathbf{B}(\mathbf{x}(t)), \quad t > 0, \\ \mathbf{x}(0) &= \mathbf{x}_0, \quad \mathbf{v}(0) = \mathbf{v}_0.\end{aligned}\tag{5.1}$$

We take two 3D vector fields $\mathbf{B}(\mathbf{x}) : \mathbf{x} \in \mathbb{R}^3 \rightarrow \mathbb{R}^3$ and $\mathbf{E}(\mathbf{x}) = -\nabla_{\mathbf{x}}\phi(\mathbf{x})$ with some $\phi(\mathbf{x}) : \mathbb{R}^3 \rightarrow \mathbb{R}$, then (5.1) is an Hamiltonian system with the energy conserved as

$$\mathcal{H}_s(t) := \frac{1}{2}|\mathbf{v}(t)|^2 + \phi(\mathbf{x}(t)) = \mathcal{H}_s(0), \quad t \geq 0.\tag{5.2}$$

Note here we do not require \mathbf{B} being divergence free for these accuracy tests, since all the presented properties of the proposed schemes hold in general as long as \mathbf{B} is a smooth enough vector field. Hence, we first focus on a constant intensity magnetic field before considering the general case to test the proposed methods MRC, TSF and MM.

Example 5.1. (*Constant intensity*). We take the two external fields in the system (5.1)

$$\mathbf{E}(\mathbf{x}) = \begin{pmatrix} \cos(x_1/2) \sin(x_2) \sin(x_3)/2 \\ \sin(x_1/2) \cos(x_2) \sin(x_3) \\ \sin(x_1/2) \sin(x_2) \cos(x_3) \end{pmatrix}, \quad \mathbf{B}(\mathbf{x}) = \begin{pmatrix} \sin(x_1 + x_2) \\ \cos(x_1 + x_2) \sin(x_3) \\ \cos(x_1 + x_2) \cos(x_3) \end{pmatrix}, \quad \mathbf{x} = (x_1, x_2, x_3),$$

where $|\mathbf{B}(\mathbf{x})| = 1$ and $\mathbf{E}(\mathbf{x})$ derives from the potential $\phi(\mathbf{x})$:

$$\mathbf{E}(\mathbf{x}) = -\nabla_{\mathbf{x}}\phi(\mathbf{x}), \quad \phi(\mathbf{x}) = -\sin(x_1/2) \sin(x_2) \sin(x_3).$$

We choose the initial data for (5.1) as

$$\mathbf{x}_0 = (1/3, -1/2, \sqrt{\pi}/2), \quad \mathbf{v}_0 = (1/2, e/4, -1/3).$$

A reference solution is obtained by using the fourth order Runge-Kutta method with small step size $\Delta t = 10^{-5}$.

We firstly study the convergence of the three proposed methods (MRC, TSF and MM) aiming to illustrate their uniform accuracy for all $\varepsilon \in]0, 1]$. To do so, we solve the system under different ε till $T = \pi/2$ and compute the error

$$error = \frac{|\mathbf{x}(T) - \mathbf{x}^{num}|}{|\mathbf{x}(T)|} + \frac{|\mathbf{v}(T) - \mathbf{v}^{num}|}{|\mathbf{v}(T)|},\tag{5.3}$$

where \mathbf{x}^{num} and \mathbf{v}^{num} are the numerical values obtained by the different schemes. For the TSF and MM methods, we define the time step $\Delta t = T/M$ with $M \in \mathbb{N}^*$ and we fix the grid points for τ -direction as $N_\tau = 32$. For MRC, we define the numerical parameters from a given $M \in \mathbb{N}^*$ as follows: $H = \varepsilon M_f/M$ and $h = 2\pi/M$ if $M_f/M \geq 1$ and $\Delta t = 2\pi/M$ if $M_f/M < 1$ (M_f being defined by (3.4)).

The error (defined by (5.3)) produced by the three methods at $T = \pi/2$ with respect to the number of (macro) grid points M or with respect to ε is given in Figure 1. As expected, the three methods enjoy the uniform second order accuracy property since the rate of convergence is essentially insensitive to the value $\varepsilon \in]0, 1]$. The typical behavior of uniformly accurate methods can be observed on the error as a function of ε : the curves obtained for different M are almost parallel. Note that the results obtained by TSF and MM are very close whereas the error produced by MRC becomes smaller when ε decreases.

In Figure 2 we look at the error of TSF and MM with respect to the number of grid points N_τ in the auxiliary variable τ (the time step is fixed to $\Delta t = 10^{-5}$). This error is important to study since these two methods involve an additional variable τ which may make them less competitive. We can see in Figure 2 that the error decreases spectrally as the number of grid points N_τ increases. Moreover, for small values of ε , a very small number of N_τ is needed to reach high accuracy: $\varepsilon \leq 2^{-7}$, $N_\tau = 16$ is enough for machine precision. Finally, let us remark that the results obtained for MM is

much less sensitive than TSF: when $\varepsilon = 1/2$, $N_\tau = 32$ enables to reach machine precision for MM whereas TSF requires $N_\tau = 128$.

We now intend to compare the efficiency of TSF, MM and MRC in different regimes ($\varepsilon = 1/2$ and $1/2^{14}$). Let us first fix the numerical parameters. According to the previous comments, in the regime $\varepsilon = 1/2$ we take $N_\tau = 128$ for TSF and $N_\tau = 32$ for MM whereas in the regime $\varepsilon = 1/2^{14}$, we take $N_\tau = 8$ for both TSF and MM. We test the long time behavior of the three methods by investigating the relative error on the numerical total energy defined by

$$\text{error}(t^n) = \frac{|\mathcal{H}_s^n - \mathcal{H}_s(0)|}{|\mathcal{H}_s(0)|}, \quad \mathcal{H}_s^n = \frac{1}{2}|\mathbf{v}^n|^2 + \phi(\mathbf{x}^n), \quad (5.4)$$

where \mathcal{H}_s^n is the numerical approximation of $\mathcal{H}_s(t_n)$ given by (5.2). We plot in Figure 3 the error (considering the maximum of (5.4) among all the iterations) against the computational time of the three methods for $\varepsilon = 1/2$ or $1/2^{14}$ (different time steps have been chosen). For a given error, when $\varepsilon = 1/2$ the MRC method is more efficient than TSF or MM, but it is no longer true when ε becomes smaller. This is explained by the fact that N_τ can be chosen smaller in the asymptotic regime, making TSF and MM more competitive. MRC for $\varepsilon = 1/2$ reads as the Strang splitting, while for $\varepsilon = 1/2^{14}$ the convergence of MRC becomes first order in terms of total computational cost. Then, in Figure 4, the time history of (5.4) is plotted for the three methods till $T = 32\pi$, for $\varepsilon = 1/2^{14}$. The TSF and MM methods run with $N_\tau = 32$ and $M = 1024$ ($\Delta t = 0.098$) or $M = 2048$ ($\Delta t = 0.049$). We report that, for this test, MM becomes unstable in large time so that the restart strategy is used every $T_0 = 8\pi$. For MRC, we used $M = 64$ or $M = 128$. Figure 4 clearly shows that MRC has the best long time behavior among the three methods. Indeed, TSF and MM has a linear drift in the energy error as time evolves whereas for MRC, it remains of the same order (about 10^{-5}) for large time. Let us remark that the energy error converges quadratically for the three methods with respect to number of time grid points M .

Finally, we consider the scheme MM ($M = 32$, $N_\tau = 32$) to illustrate the reconstruction of the whole trajectory for $t \in [0, \pi]$ (so that $\Delta t = 0.0982$). To do so, we still consider the system (5.1) with example 5.1, with $\varepsilon = 1/2^5$. In Figure 5, we plot a reference trajectory (obtained with a very small time step) and the numerical solution obtained by MM using the strategy proposed in Section 3.3 (i.e. with a coarse time grid and using the linear interpolation strategy in (3.27)). Using a few grid points, we can see that the MM method is able to fully restore the complex trajectory (highly oscillatory confined behavior around magnetic field line) of the particle under trivial computational cost.

Example 5.2. (*Varying intensity*) Secondly, we investigate the numerical performance of the strategy proposed in Section 4 for a magnetic field with varying direction and varying intensity on the particle system (5.1).

We shall consider the particle system (5.1) with the same electric field $\mathbf{E}(\mathbf{x})$ as before, but here the magnetic field is

$$\mathbf{B}(\mathbf{x}) = \begin{pmatrix} 1 - \sin(x_2)/2 \\ 1 + \cos(x_3)/2 \\ 1 + \cos(x_1)/2 \end{pmatrix}, \quad \mathbf{x} = (x_1, x_2, x_3),$$

which satisfies $\nabla_{\mathbf{x}} \cdot \mathbf{B} = 0$ but has a varying intensity in $\mathbf{x} \in \mathbb{R}^3$ since

$$|\mathbf{B}(\mathbf{x})|^2 = 3 + \cos(x_1) + \cos(x_3) - \sin(x_2) + \cos(x_1)^2/4 + \sin(x_2)^2/4 + \cos(x_3)^2/4.$$

We choose the same initial data as before for example 5.1 and solve the problem via the new time formulation (4.2) with the MM method (see Section 4). The reference solution is again obtained by directly solving (5.1) with the fourth order Runge-Kutta method under small step size ($\Delta t = 10^{-5}$).

First, we are interested in the error (defined by (5.3)) against the number of grid points M for the quantities $\mathbf{x}(t)$, $\mathbf{v}_\parallel(t) := \mathbf{v}(t) \cdot \mathbf{B}(\mathbf{x}(t))\mathbf{B}(\mathbf{x}(t))/\|\mathbf{B}(\mathbf{x}(t))\|^2$ and $|\mathbf{v}(t)|$ at $T = 1$. In Figure 6, we can observe that the proposed MM scheme converges as number grid points M increases (Δs decreases) with uniform second order accurate rate for all $\varepsilon \in]0, 1]$.

Then, in Figure 7, the time history of the energy error (defined by (5.4)) of the method with $\Delta s = 1/8$ and $\Delta s = 1/16$ till a physical time $T = T(s) = 100$ and under three different ε is shown.

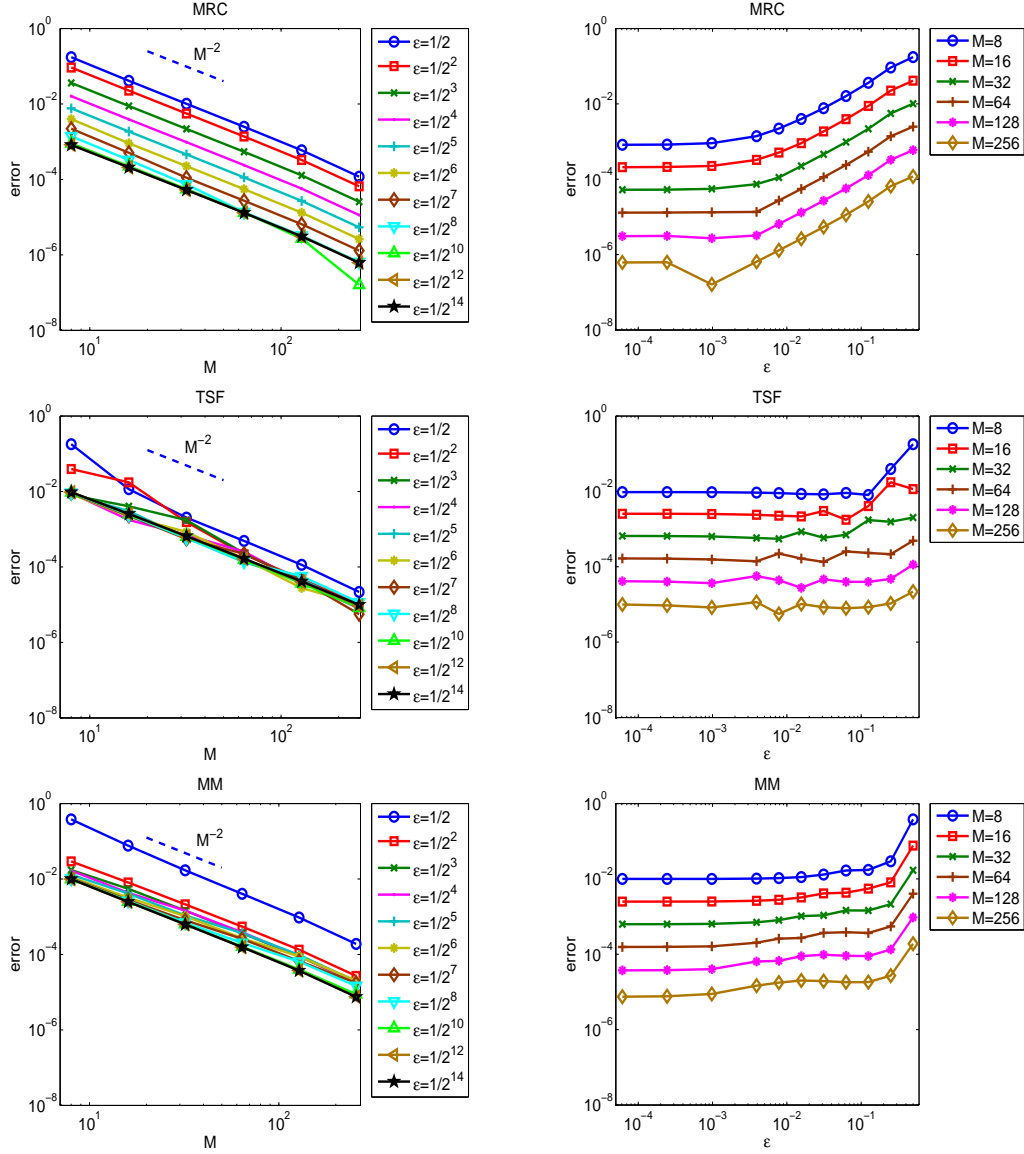


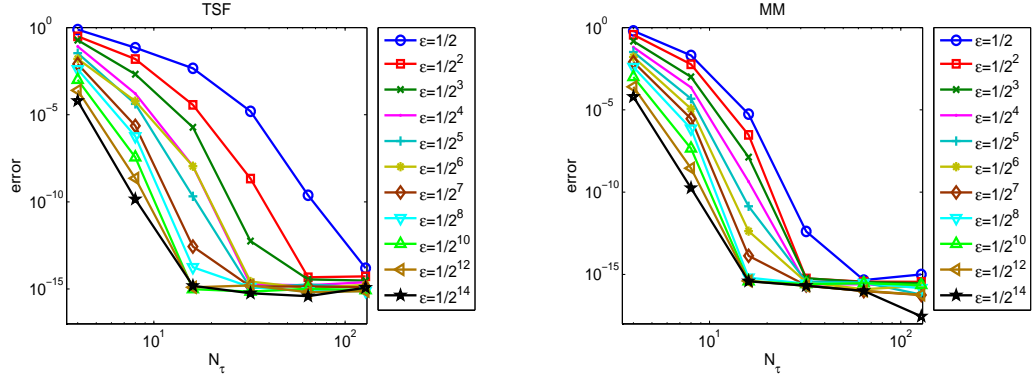
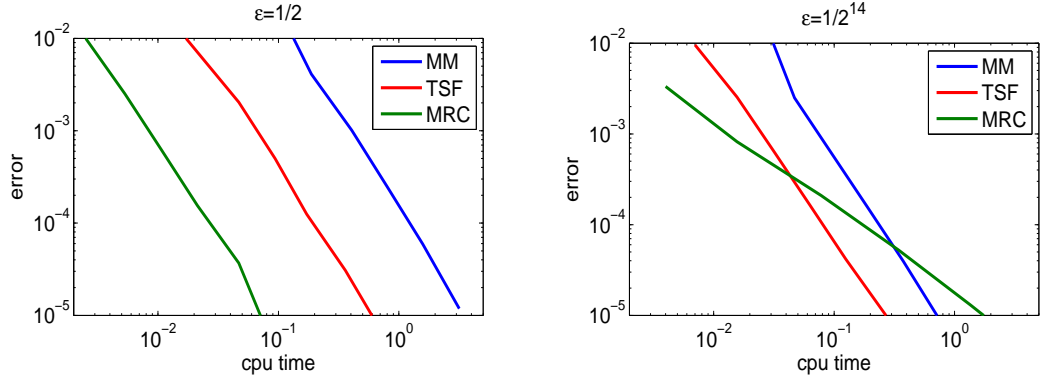
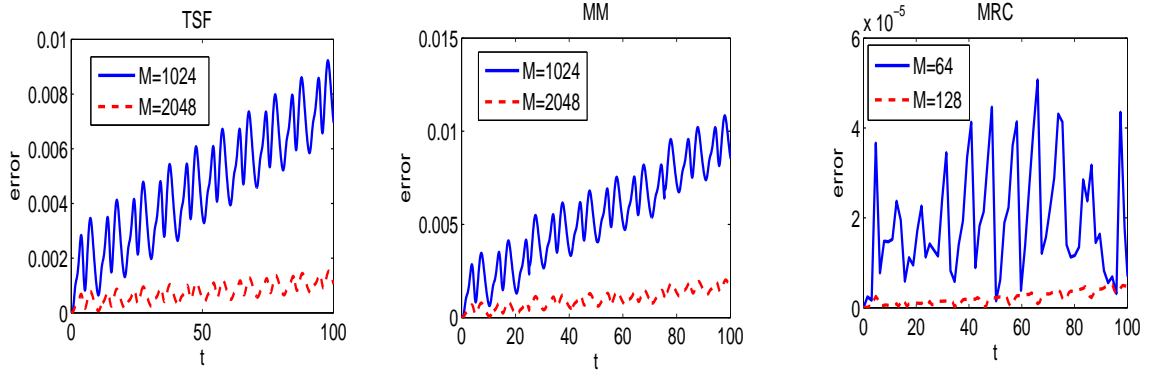
FIGURE 1. Errors of MRC, TSF and MM with respect to time steps M under different ε (left) or with respect to ε under different M (right) for example 5.1.

Let us remark that the restart strategy is used at every time step. In Figure 7, we observe that the scheme computes the energy (5.2) with uniform second order accuracy for $\varepsilon \in]0, 1]$. Under a rather large step size ($\Delta s \gg \varepsilon$), the scheme is stable in long time computing, and even if a slight linear drift in the energy error is observed, the energy error (about 10^{-3}) is rather good for all ε considered. In Figure 7, the relation between the new time s and the physical time $t(s)$ is also plotted to illustrate that the physical time $t(s)$ is a monotone increasing function.

Finally, we study the dynamics of the magnetic moment defined by

$$I(t) = \frac{1}{2} \frac{|\mathbf{v}_\perp(t)|^2}{|\mathbf{B}(\mathbf{x}(t))|}, \quad (5.5)$$

which is an analogy of (4.7) at the particle level (5.1). We use MM with $\Delta s = 1/16$ (so that it is accurate enough) to solve (5.1) till $t = 100$ with three different values of ε ($\varepsilon = 2^{-9}, 2^{-10}, 2^{-11}$).

FIGURE 2. Error of TSF and MM with respect to N_τ under different ε for example 5.1.FIGURE 3. Efficiency comparison of TSF, MM and MRC in classical (left) or asymptotic regime (right) of ε for example 5.1: error versus computational time.FIGURE 4. Energy error of TSF, MM (with restart every $T_0 = 8\pi$) and MRC for example 5.1 under $\varepsilon = 1/2^{14}$ till $T = 32\pi$. $\Delta t = 0.0982$ or 0.0491 for TSF and MM.

In Figure 8, the relative error on the magnetic moment, i.e. $|I(t_n) - I(0)|/(\varepsilon I(0))$ is displayed as a function of the rescaled time s . Let us remark that the MM scheme captures this quantity $I(t)$ with uniform second order accuracy for $\varepsilon \in]0, 1]$, since $I(t)$ only depends on $|\mathbf{v}|$ and \mathbf{v}_\parallel through

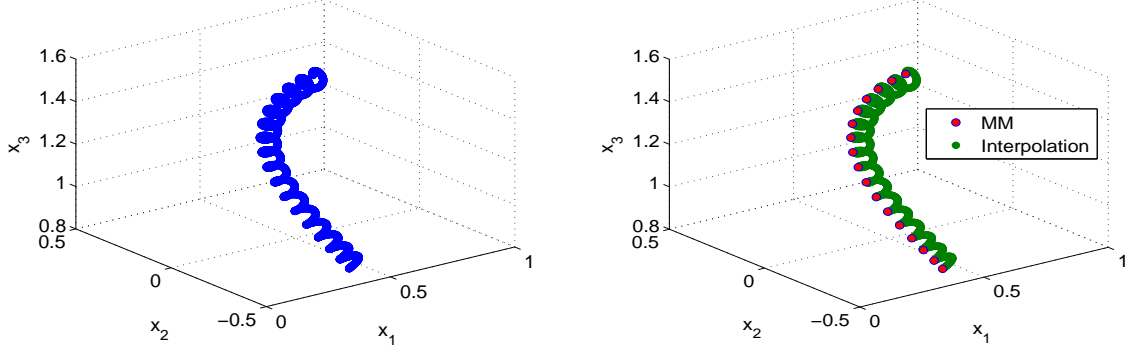


FIGURE 5. Left: exact trajectory of the particle in example 5.1 till $T = \pi$ under $\varepsilon = 1/2^5$. Right: numerical solution of MM under $\Delta t = 0.0982$ (red curve) and the fully recovered trajectory with fine linear interpolation.

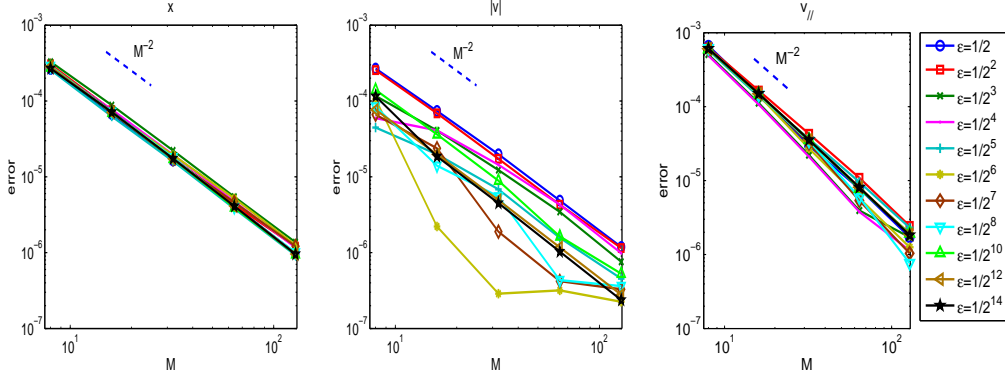


FIGURE 6. Error of MM under different $M = \Delta s^{-1}$ in \mathbf{x} , $|\mathbf{v}|$ and v_{\parallel} at $T = 1$ in example 5.2 of varying intensity.

$|\mathbf{v}_{\perp}|^2 = |\mathbf{v}|^2 - |v_{\parallel}|^2$. The deviation of the magnetic moment (5.5) behaves as $|I(t) - I(0)| = O(\varepsilon)$ in the simulation, which is consistent with the results obtained in [25]. Our scheme captures this adiabatic quantity even when $\Delta s \gg \varepsilon$ whereas the scheme used in [25] needs $\Delta s < \varepsilon$.

5.2. Simulation of the Vlasov-Poisson system. In this last part, we focus on the numerical simulation of the full 3D Vlasov-Poisson equation (1.1) using the MRC method. The chosen initial data is a Maxwellian in velocity and a ring-shape distribution in space with a perturbation in angle [17]:

$$f_0(\mathbf{x}, \mathbf{v}) = \frac{n_0}{2\pi} (1 + \eta \cos(k\theta)) e^{-5(r-5)^2} e^{-\frac{1}{2}|\mathbf{v}|^2}, \quad (5.6)$$

where $\mathbf{x} = (x_1, x_2, x_3)$, $\mathbf{v} = (v_1, v_2, v_3)$, $r = |\mathbf{x}|$ and $\theta = \arctan(x_2/x_1)$. The non-homogenous magnetic field is taken as in [29] (screw-pinch setup)

$$\mathbf{B}(\mathbf{x}) = \frac{1}{\sqrt{1 + \alpha^2 x_1^2 + \alpha^2 x_2^2}} \begin{pmatrix} \alpha x_2 \\ -\alpha x_1 \\ 1 \end{pmatrix},$$

which satisfies both $|\mathbf{B}(\mathbf{x})| = 1$ and $\nabla_{\mathbf{x}} \cdot \mathbf{B}(\mathbf{x}) = 0$. The spatial domain is a cartesian geometry $\mathbf{x} = (x_1, x_2, x_3) \in \Omega = [-8, 8] \times [-8, 8] \times [0, 1]$. We choose $n_0 = 100$, $\eta = 0.05$, $k = 4$ and discretize the spatial domain Ω with $N_{x_1} = N_{x_2} = 256$ points in x_1, x_2 -directions and $N_{x_3} = 4$ points in

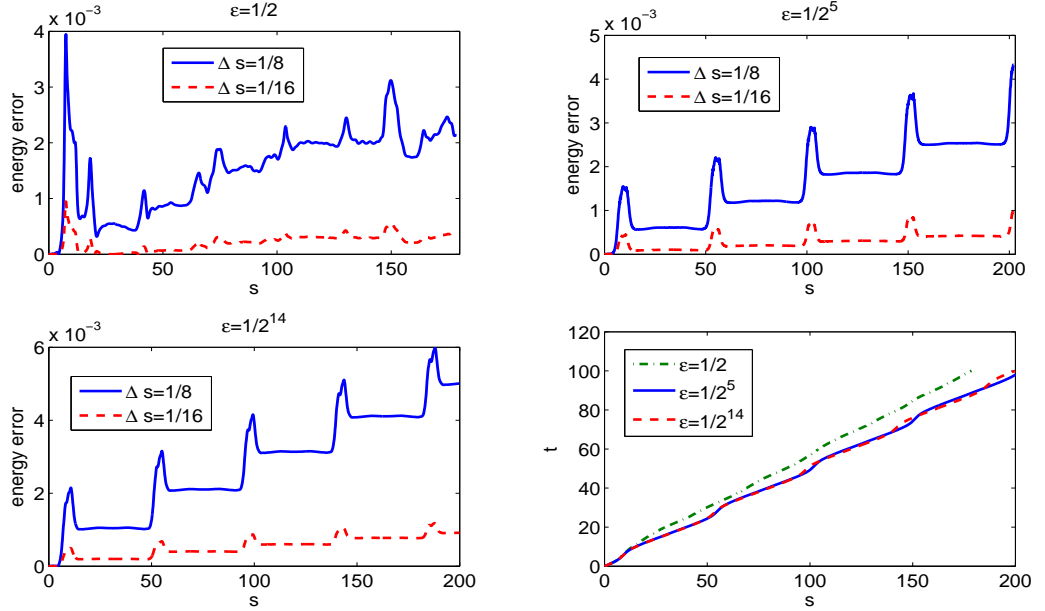


FIGURE 7. Energy error of MM (restart each step) for $\varepsilon = 1/2, 1/2^5, 1/2^{14}$ till $t = 100$ and the evolution of $t(s)$ in example 5.2.

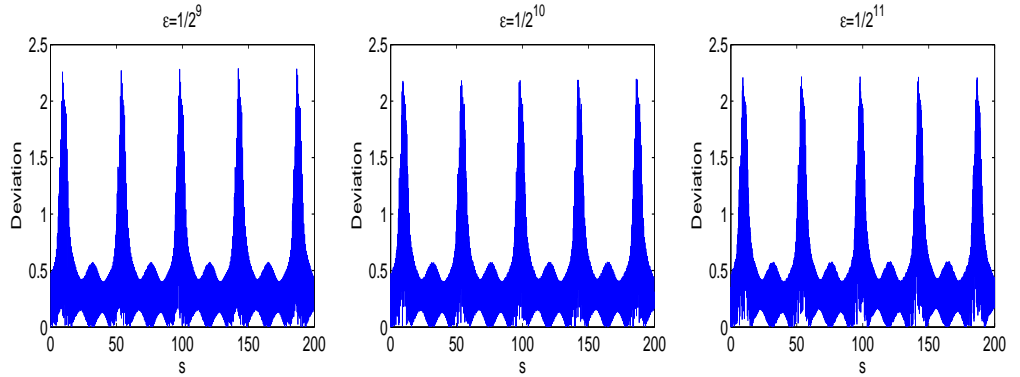


FIGURE 8. Deviation of the magnetic moment: $\frac{1}{\varepsilon} |I(t) - I(0)|/I(0)$ till $t = 100$ in example 5.2 under different ε (computed with $\Delta s = 1/16 \gg \varepsilon$).

x_3 -direction. As a diagnostic, we consider the following quantity:

$$\rho^\varepsilon(t, \mathbf{x}) = \int_{\mathbb{R}^3} f^\varepsilon(t, \mathbf{x}, \mathbf{v}) d\mathbf{v}, \quad \mathbf{x} \in \Omega.$$

For the PIC method, we choose $N_p = 100 \times N_{x_1} N_{x_2} N_{x_3}$ particles and the projection of the particles on the spatial grid is done by cubic splines.

In Figures 9, the density ρ^ε is displayed at different times for $\varepsilon = 1/2^5$ with $M = 256$ whereas $\alpha = 0$ in the magnetic field, so that \mathbf{B} is homogeneous and aligned with the x_3 direction. There is two different dynamics which can be seen in the results: an instability develops in the direction orthogonal to the magnetic field (one can see four vortices at time $t = 64\pi$) and a slight parallel dynamics in the plane parallel to the magnetic field. In Figures 10 and 11, a non-homogeneous magnetic field is considered ($\alpha = 0.003$). We can observe that the dynamics is different dynamics

from the homogeneous case. Indeed, the instability leading to the formation of four vortices is different and one can see stronger non homogeneous phenomena in the x_3 direction due to the expression of the magnetic field.

Finally, in Figure 12, we plot the energy error for both configurations ($\alpha = 0$ and $\alpha = 0.003$). Very good conservations are obtained for long time. Moreover, we consider the relative error between the Vlasov-Poisson system (1.1) and the asymptotic model (2.4) as a function of ε , for $\alpha = 0.003$. To do so, we compute the L^∞ norm (in space) of $|\rho^\varepsilon(t = \pi, \mathbf{x}) - \rho(t = \pi, \mathbf{x})|/|\rho^\varepsilon(t = \pi, \mathbf{x})|$ at the final time $t = \pi$. We can see that when ε decreases, the error is $O(\varepsilon)$, as predicted by the theory.

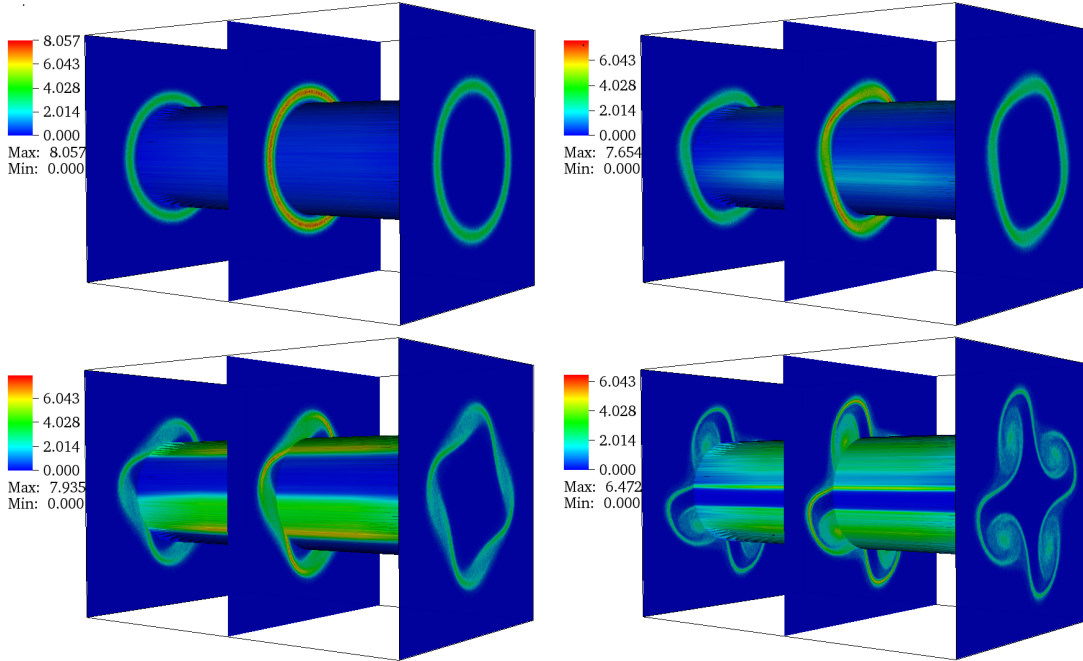


FIGURE 9. Vlasov-Poisson case: pseudo-color snapshots of ρ^ε under $\varepsilon = 1/2^5$ at $t = 0, 16\pi, 32\pi, 64\pi$ with initial condition 5.6 with $\alpha = 0$.

ACKNOWLEDGEMENTS

This work is supported by the French ANR project MOONRISE ANR-14-CE23-0007-01. This work has been carried out within the framework of the French Federation for Magnetic Fusion Studies (FR-FCM) and of the Eurofusion consortium, and has received funding from the Euratom research and training programme 2014-2018 and 2019-2020 under grant agreement No 633053. The views and opinions expressed herein do not necessarily reflect those of the European Commission.

REFERENCES

- [1] A. ABDULLE, W. E. B. ENGQUIST, E. VANDEN-ELJNDEN, The heterogeneous multiscale method, *Acta Numer.* 21 (2012) pp. 1-87.
- [2] C.K. BIRDSALL, A.B. LANGDON, *Plasma Physics via Computer Simulation*, Adam Hilger, 1991.
- [3] M. BOSTAN, The Vlasov-Maxwell system with strong initial magnetic field. Guiding-center approximation, *SIAM J. Multiscale Model. Simul.* 6 (2007), pp.1026-1058.
- [4] M. BOSTAN, A. FINOT, The effective Vlasov-Poisson system for the finite Larmor radius regime, *SIAM J. Multiscale Model. Simul.* 14 (2015), pp. 1238-1275.
- [5] PH. CHARTIER, N. CROUSEILLES, M. LEMOU, An averaging technique for transport equations, arXiv:1609.09819v1, preprint, 2018.
- [6] PH. CHARTIER, N. CROUSEILLES, M. LEMOU, F. MÉHATS, Uniformly accurate numerical schemes for highly oscillatory Klein-Gordon and nonlinear Schrödinger equations, *Numer. Math.* 129 (2015), pp. 211-250.

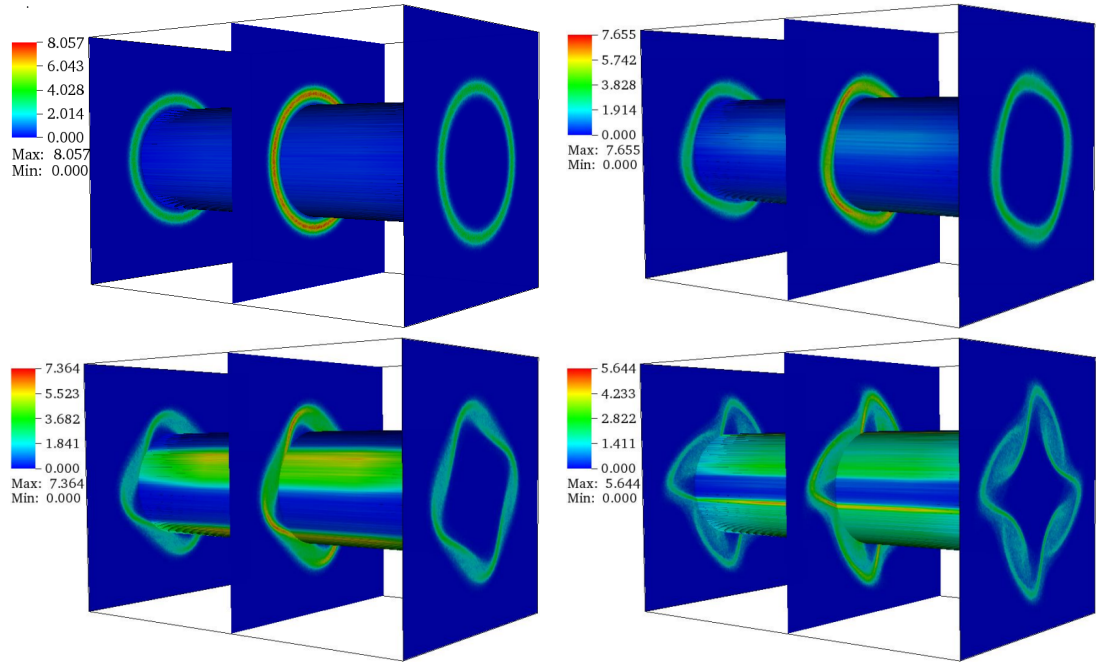


FIGURE 10. Vlasov-Poisson case: pseudo-color snapshots of ρ^ε under $\varepsilon = 1/2^5$ at $t = 0, 16\pi, 32\pi, 64\pi$ with initial condition 5.6 with $\alpha = 0.003$.

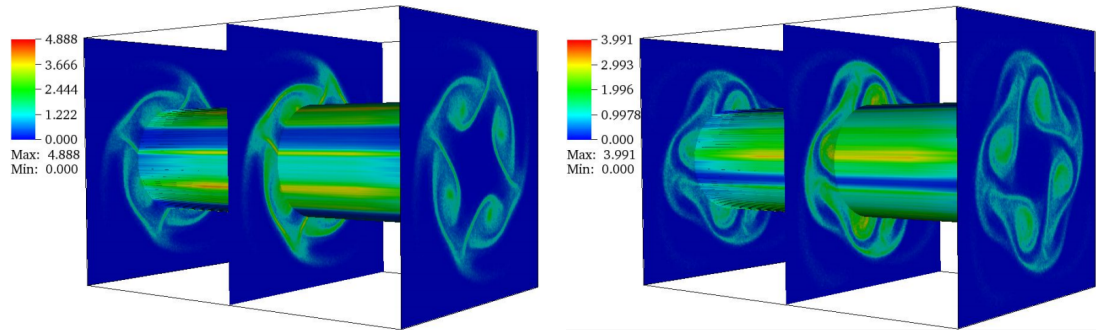


FIGURE 11. Vlasov-Poisson case: pseudo-color snapshots of ρ^ε under $\varepsilon = 1/2^5$ at $t = 88\pi, 128\pi$ with initial condition 5.6 with $\alpha = 0.003$.

- [7] PH. CHARTIER, M. LEMOU, F. MÉHATS, G. VILMART, A new class of uniformly accurate methods for highly oscillatory evolution equations, hal-01666472, 2017.
- [8] PH. CHARTIER, J. MAKAZAGA, A. MURUA, G. VILMART, Multi-revolution composition methods for highly oscillatory differential equations, Numer. Math. 128 (2014), pp 167-192.
- [9] PH. CHARTIER, F. MÉHATS, M. THALHAMMER, Y. ZHANG, Convergence analysis of multi-revolution composition time-splitting pseudo-spectral methods for highly oscillatory differential equations of Schrödinger equations, ESAIM:M2AN 51 (2017) pp. 1859-1882.
- [10] PH. CHARTIER, N. CROUSEILLES, M. LEMOU, F. MÉHATS, X. ZHAO, Uniformly accurate methods for Vlasov equations with non-homogeneous strong magnetic field, to appear on Math. Comp. (2019).
- [11] PH. CHARTIER, N. CROUSEILLES, X. ZHAO, Numerical methods for the two-dimensional Vlasov-Poisson equation in the finite Larmor radius approximation regime, J. Comput. Phys. 375 (2018) pp. 619-640.
- [12] N. CROUSEILLES, M. LEMOU, F. MÉHATS, Asymptotic preserving schemes for highly oscillatory Vlasov-Poisson equations, J. Comput. Phys. 248 (2013) pp. 287-308.

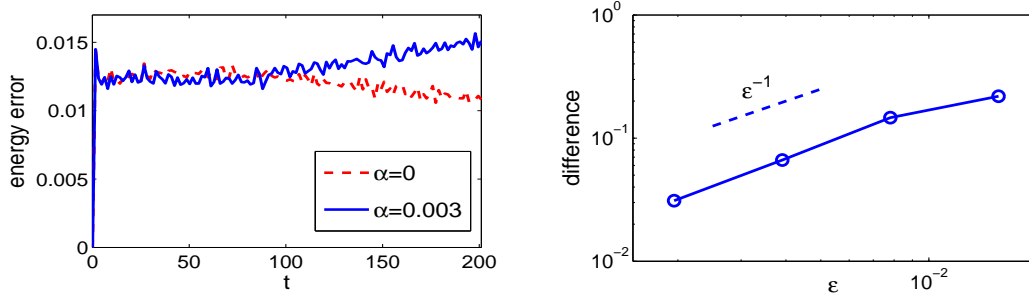


FIGURE 12. Vlasov-Poisson case. Left: time history of the energy error with initial condition 5.6. Right: difference between (1.1) and the limit model (2.4) (maximum error of $|\rho^\varepsilon(t = \pi, \mathbf{x}) - \rho(t = \pi, \mathbf{x})|/|\rho^\varepsilon(t = \pi, \mathbf{x})|$).

- [13] N. CROUSEILLES, M. LEMOU, F. MÉHATS, X. ZHAO, Uniformly accurate forward semi-Lagrangian methods for highly oscillatory Vlasov-Poisson equations, *SIAM J. Multiscale Model. Simul.* 15 (2017), pp. 723-744.
- [14] N. CROUSEILLES, S.A. HIRSTOAGA, X. ZHAO, Multiscale Particle-In-Cell methods and comparisons for long time two-dimensional Vlasov-Poisson equation with strong magnetic field, *Comput. Phys. Commun.* 222, pp. 136-151 (2018).
- [15] N. CROUSEILLES, M. LEMOU, F. MÉHATS, X. ZHAO, Uniformly accurate Particle-in-Cell method for the long time two-dimensional Vlasov-Poisson equation with uniform strong magnetic field, *J. Comput. Phys.* 346 (2017), pp. 172-190.
- [16] P. DEGOND, F. FILBET, On the asymptotic limit of the three dimensional Vlasov-Poisson system for large magnetic field: formal derivation, *J. Stat. Physicists.* 65 (2016), pp. 765-784.
- [17] F. FILBET, C. YANG, Numerical simulations to the Vlasov-Poisson system with a strong magnetic field, preprint, (2018).
- [18] F. FILBET, T. XIONG, E. SONNENDRÜCKER, On the Vlasov-Maxwell system with a strong magnetic field, *SIAM J. Applied Mathematics* 78 (2018), pp. 1030-1055.
- [19] F. FILBET, M. RODRIGUES, Asymptotically stable particle-in-cell methods for the Vlasov-Poisson system with a strong external magnetic field, *SIAM J. Numer. Anal.* 54 (2016), pp. 1120-1146.
- [20] F. FILBET, M. RODRIGUES, Asymptotically preserving particle-in-cell methods for inhomogeneous strongly magnetized plasmas, *SIAM J. Numer. Anal.* 55 (2017), pp. 2416-2443.
- [21] E. FRÉNOT, F. SALVARANI AND E. SONNENDRÜCKER, Long time simulation of a beam in a periodic focusing channel via a two-scale PIC-method, *Math. Models Methods Appl. Sci.* 19 (2009), pp. 175-197.
- [22] E. FRÉNOT, E. SONNENDRÜCKER, Long time behavior of the two-dimensional Vlasov equation with a strong external magnetic field, *Math. Models Methods Appl. Sci.* 10 (2000), pp. 539-553.
- [23] E. FRÉNOT, S.A. HIRSTOAGA, M. LUTZ, E. SONNENDRÜCKER, Long time behavior of an exponential integrator for a Vlasov-Poisson system with strong magnetic field, *Commun. in Comput. Phys.* 18 (2015), pp. 263-296.
- [24] F. GOLSE, L. SAINT-RAYMOND, The Vlasov-Poisson system with strong magnetic field, *J. Math. Pures Appl.* 78 (1999), pp. 791-817.
- [25] E. HAIRER, CH. LUBICH, Long-term analysis of a variational integrator for charged-particle dynamics in a strong magnetic field, preprint 2018.
- [26] G.B. JACOBS, J.S. HESTHAVEN, Implicit-Explicit time integration of a high-order particle-in-cell method with hyperbolic divergence cleaning, *Comput. Phys. Comm.* 180 (2009), pp. 1760-1767.
- [27] S. JIN, Efficient asymptotic-preserving (AP) schemes for some multiscale kinetic equations, *SIAM J. Sci. Comput.* 21 (1999), pp. 441-454.
- [28] M. KRAUS, K. KORMANN, P. MORRISON, E. SONNENDRÜCKER, GEMPIC: geometric electromagnetic Particle In Cell methods, *Journal of Plasma Physics* 83 (4), (2017)
- [29] G. LATU, M. MEHRENBARGER, Y. GÜÇLÜ, M. OTTAVIANI, E. SONNENDRÜCKER, Field-Aligned Interpolation for Semi-Lagrangian Gyrokinetic Simulations, *J. Sci. Comput.* 74 (2018), pp. 1601-1650.
- [30] W.W. LEE, Gyrokinetic approach in particle simulation, *Phys. Fluids* 26 (1983).
- [31] T.G. NORTHROP, The adiabatic motion of charged particles. *Interscience Tracts on Physics and Astronomy*, Vol. 21. Interscience Publishers John Wiley & Sons New York-London-Sydney, 1963.
- [32] H. QIN ET AL, Canonical symplectic particle-in-cell method for long-term large-scale simulations of the Vlasov-Maxwell system, *Nucl. Fusion*, 56, 014001 (2016).
- [33] L. SAINT-RAYMOND, The gyro-kinetic approximation for the Vlasov-Poisson system, *Math. Models Methods Appl. Sci.* 10 (2000), pp. 1305-1332.
- [34] J.A. SANDERS, F. VERHULST, Averaging methods in nonlinear dynamical systems, volume 59 of *Applied Mathematical Sciences*. Springer-Verlag, New York, 1985.

[35] E. SONNENDRÜCKER, Numerical Methods for Vlasov Equations, Lecture notes, 2016.

PH. CHARTIER: UNIV RENNES, INRIA-MINGUS, CNRS, IRMAR-UMR 6625, F-35000 RENNES, FRANCE
E-mail address: `Philippe.Chartier@inria.fr`

N. CROUSEILLES: UNIV RENNES, INRIA-MINGUS, CNRS, IRMAR-UMR 6625, F-35000 RENNES, FRANCE
E-mail address: `nicolas.crouseilles@inria.fr`

M. LEMOU: UNIV RENNES, CNRS, INRIA-MINGUS, IRMAR-UMR 6625, F-35000 RENNES, FRANCE
E-mail address: `mohammed.lemou@univ-rennes1.fr`

F. MÉHATS: UNIV RENNES, INRIA-MINGUS, CNRS, IRMAR-UMR 6625, F-35000 RENNES, FRANCE
E-mail address: `florian.mehats@univ-rennes1.fr`

X. ZHAO: SCHOOL OF MATHEMATICS AND STATISTICS, WUHAN UNIVERSITY, 430072 WUHAN, CHINA; UNIV RENNES,
INRIA-MINGUS, CNRS, IRMAR-UMR 6625, F-35000 RENNES, FRANCE
E-mail address: `zhxfnus@gmail.com`